Available online at www.sciencedirect.com

ScienceDirect

Geochimica et Cosmochimica Acta xxx (2022) xxx–xxx

Geochimica et Cosmochimica Acta

www.elsevier.com/locate/gca

Triple oxygen isotope distribution in modern mammal teeth and potential geologic applications

Sophie B. Lehmann [a,*,1], Naomi E. Levin [b,*], Benjamin H. Passey [b], Huanting Hu [c], Thure E. Cerling [d,e], Joshua H. Miller [f], Laura Arppe [g], Emily J. Beverly [h], Kathryn A. Hoppe [i,j], Tyler E. Huth [b], Julia R. Kelson [b], Julie Luyt [k], Judith Sealy [k]

[a] *Morton K. Blaustein Department of Earth and Planetary Sciences, The Johns Hopkins University, 301 Olin Hall, 3400 N. Charles Street, Baltimore, MD 21218, USA*

[b] *Department of Earth and Environmental Sciences, University of Michigan, 1100 North University Avenue, Ann Arbor, MI 48109, USA*

[c] *School of Oceanography, Shanghai Jiao Tong University, China*

[d] *Department of Biology, University of Utah, Salt Lake City, UT 84112, USA*

[e] *Department of Geology and Geophysics, University of Utah, Salt Lake City, UT 84112, USA*

[f] *Department of Geology, University of Cincinnati, Cincinnati, OH 45221, USA*

[g] *Finnish Museum of Natural History, University of Helsinki, Helsinki, Finland*

[h] *Department of Earth and Atmospheric Sciences, University of Houston, Houston, TX 77204, USA*

[i] *Green River College, University of Washington, USA*

[j] *Burke Museum, University of Washington, USA*

[k] *Department of Archaeology, University of Cape Town, South Africa*

Received 10 March 2021; accepted in revised form 28 April 2022; available online xxxx

Abstract

Reconstructing water availability in terrestrial ecosystems is key to understanding past climate and landscapes, but there are few proxies for aridity that are available for use at terrestrial sites across the Cenozoic. The isotopic composition of tooth enamel is widely used as a paleoenvironmental indicator and recent work suggests the potential for using the triple oxygen isotopic composition of the carbonate component of mammalian tooth enamel ($\Delta'^{17}O_{enamel}$) as an indicator of aridity. However, the extent to which $\Delta'^{17}O_{enamel}$ values vary across environments is unknown and there is no framework for evaluating past aridity using $\Delta'^{17}O_{enamel}$ data. Here we present $\Delta'^{17}O_{enamel}$ and $\delta^{18}O_{enamel}$ values from 50 extant mammalian herbivores that vary in physiology, behavior, diet, and water-use strategy. Teeth are from sites in Africa, Europe, and North America and represent a range of environments (humid to arid) and latitudes (34°S to 69°N), where mean annual $\delta^{18}O$ values of meteoric water range from –26.0‰ to 2.2‰ (VSMOW). $\Delta'^{17}O_{enamel}$ values from these sites span 162 per meg (–252 to –90 per meg), where 1 per meg = 0.001‰). The observed variation in $\Delta'^{17}O_{enamel}$ values increases with aridity, forming a wedge-shaped pattern in a plot of aridity index vs. $\Delta'^{17}O_{enamel}$ that persists regardless of geographic region. In contrast, the plot of aridity index vs. $\delta^{18}O_{enamel}$ for these same samples does not yield a distinct pattern. We use these new $\Delta'^{17}O_{enamel}$ data from extant teeth to provide guidelines for using $\Delta'^{17}O_{enamel}$ data from fossil teeth to assess and classify the aridity of past environments. $\Delta'^{17}O_{enamel}$ values from the fossil record have the potential to be a widely used proxy for aridity without the limitations inherent to approaches that use $\delta^{18}O_{enamel}$ values alone. In addition, the data presented here have implications for how

* Corresponding authors.

E-mail addresses: sophie.b.lehmann@gmail.com (S.B. Lehmann), nelevin@umich.edu (N.E. Levin), passey@umich.edu (B.H. Passey), huanting.hu@sjtu.edu.cn (H. Hu), thure.cerling@utah.edu (T.E. Cerling), josh.miller@uc.edu (J.H. Miller), laura.arppe@helsinki.fi (L. Arppe), ejbeverly@uh.edu (E.J. Beverly), khoppe@greenriver.edu (K.A. Hoppe), tehuth@umich.edu (T.E. Huth), jrkelson@umich.edu (J.R. Kelson), Julie.luyt@uct.ac.za (J. Luyt), Judith.Sealy@uct.ac.za (J. Sealy).

[1] Present address: Department of Geology and Environmental Science, University of Pittsburgh, Pittsburgh, PA 15260, USA.

https://doi.org/10.1016/j.gca.2022.04.033

$\Delta'^{17}O_{enamel}$ values of large mammalian herbivores can be used in evaluations of diagenesis and past pCO_2 and past gross primary productivity.

Keywords: Aridity; Mammalian teeth; Paleoclimate; Environment; Stable isotopes; Triple oxygen isotopes

1. INTRODUCTION AND BACKGROUND

1.1. Traditional use of oxygen isotopes in tooth enamel as climatic and environmental proxies

The distribution of oxygen isotopes in marine and terrestrial carbonates (e.g., foraminifera tests, soil and lake carbonates, tooth enamel) has long been used to reconstruct climate, environment, and surface processes (e.g., Zachos et al., 2001; Rowley and Currie, 2006; Blumenthal et al., 2017). Oxygen isotope values ($\delta^{18}O$) of carbonate vary with environmental conditions and geography because they reflect the $\delta^{18}O$ value of the waters from which they form. The $\delta^{18}O$ value of meteoric-derived waters (e.g., rain, rivers, lakes, groundwater) varies relative to climate and hydrology because it is sensitive to both equilibrium (e.g., temperature changes, Rayleigh distillation) and kinetic (e.g., evaporation) oxygen isotope fractionation effects (e.g., Rozanski et al., 1993). However, the influence of these isotope effects on $\delta^{18}O$ values can be difficult to tease apart.

Fossil mammalian teeth are found globally, span the Cenozoic, and are used as environmental indicators. The $\delta^{18}O$ value of tooth enamel ($\delta^{18}O_{enamel}$) is an alluring climate proxy because it often tracks $\delta^{18}O$ values of meteoric water, but this relationship is sensitive to an animal's diet, physiology, and water-use strategy (Kohn, 1996). An individual's $\delta^{18}O_{enamel}$ values and their use as paleoclimate indicators are impacted by a variety of factors, including the animal's intake of atmospheric O_2 (accounting for 5–40% of oxygen in body water), its water-use efficiency, and the degree of evaporation of ingested waters (plant waters, surface waters) relative to local precipitation. Because $\delta^{18}O_{enamel}$ values have a variety of influences, they have been used to track a range of processes. Some studies estimate changes in paleotemperature from $\delta^{18}O_{enamel}$ values, relying on the assumption that $\delta^{18}O_{enamel}$ values track the $\delta^{18}O$ value of meteoric water, which varies with temperature at mid to high latitudes (e.g., Fricke et al., 1995). However, this approach does not account for variability in $\delta^{18}O$ values of ingested waters within an ecosystem, where leaf and drinking waters can be several per mil (‰) higher than unevaporated meteoric water. Other approaches leverage these differences in evaporation and use $\delta^{18}O_{enamel}$ values from animals with different diets and behaviors to separate the influence of evaporative enrichment on $\delta^{18}O_{enamel}$ values in order to estimate past aridity (Levin et al., 2006; Blumenthal et al., 2017). This "aridity index" approach categorizes animals by their water-use strategy where evaporation-insensitive taxa, like Hippopotamidae, ingest a relatively large amount of drinking water, in contrast to evaporation-sensitive taxa, like Giraffidae, which require less drinking water. The offset between $\delta^{18}O_{enamel}$ values of evaporation-sensitive and evaporation-insensitive taxa increases with aridity. While the $\delta^{18}O_{enamel}$ aridity indicator is powerful, it is tuned to Quaternary mammal assemblages in eastern Africa (Blumenthal et al., 2017) and not easily transferrable to older periods or different regions without making assumptions about animal behavior and physiology.

1.2. Triple oxygen isotopic composition of waters and carbonates

Triple oxygen isotope (^{18}O, ^{17}O, ^{16}O) distributions in water and near-surface minerals (e.g., carbonate, gypsum) have potential as indicators of aridity because they are sensitive to kinetic isotope effects and can track the influence of evaporation (Barkan and Luz, 2005; 2007; Li et al., 2017; Surma et al., 2018; Passey and Levin, 2021).

The majority of processes involving oxygen isotopic fractionation on Earth are mass dependent and governed by the power law relationship.

$$^{17}\alpha_{a-b} = {}^{18}\alpha_{a-b}{}^{\theta}, \quad (1)$$

where the isotopic fractionation between two materials or phases, a and b, is defined as $\alpha_{a\text{-}b} = R_a/R_b$ and R represents the ratio of the heavy to light isotope ($^{18}O/^{16}O$, $^{17}O/^{16}O$) (Matsuhisa et al., 1978; Young et al., 2002). Although these relationships have been well known for more than 60 years (Craig, 1957), differences in the exponent θ were considered too small to detect with most analytical approaches and there was little motivation for analyzing $\delta^{17}O$ as it provided the same information as $\delta^{18}O$. However, efforts to increase analytical precision showed that there were measurable distinctions in θ between kinetic and equilibrium fractionation processes. These distinctions are particularly evident in the hydrosphere where θ is 0.529 for equilibrium exchange between water liquid and vapor, but 0.5185 for the diffusion of water through air that occurs during evaporation (Young et al., 2002; Barkan and Luz, 2005; 2007).

These θ values are equivalent to the slope on a $\delta'^{18}O$ - $\delta'^{17}O$ plot, where

$$\delta^{x}O_x = \left(\frac{R_{sample}}{R_{standard}} - 1\right) * 1000, \quad (2)$$

and

$$\delta'^{x}O_x = \ln\left(\frac{R_{sample}}{R_{standard}}\right), \quad (3)$$

and x = 17 or 18. Given the small distinctions in slope that differentiate equilibrium and kinetic fractionation (0.529 vs. 0.5185), we use $\Delta'^{17}O$ to visualize and discuss triple oxygen isotope variation, where

$$\Delta'^{17}O = \delta'^{17}O - \lambda_{RL} * \delta'^{18}O, \quad (4)$$

Please cite this article in press as: Lehmann S. B., et al. Triple oxygen isotope distribution in modern mammal teeth and potential geologic applications. *Geochim. Cosmochim. Acta* (2022), https://doi.org/10.1016/j.gca.2022.04.033

where λ_{RL} represents the slope of the reference line in the $\delta'^{18}O$ - $\delta'^{17}O$ plot and is the mathematical equivalent to θ as defined in Eq. (1) (Miller, 2002). For this study we use a λ_{RL} of 0.528 which is consistent with the literature reporting $\Delta'^{17}O$ values in applications to the hydrosphere and in many geological studies (e.g., Barkan and Luz, 2005; Schoenemann et al., 2013; Passey et al., 2014; Sharp and Wostbrock, 2021). Larger deviations and more negative $\Delta'^{17}O$ values reflect a greater influence of evaporation (Figs. 1–2).

Meteoric-derived waters like rain, river, lake, and ground waters have $\Delta'^{17}O$ values that range from –56 to +60 per meg (Landais et al., 2006, 2010; Barkan and Luz, 2011; Surma et al., 2015, 2018; Li et al., 2017; Passey and Ji, 2019; Uechi and Uemura, 2019). However, exceptions include evaporated ponds in the Atacama Desert and in the Sistan Oasis that yield much lower $\Delta'^{17}O$ values (∼−70 per meg and −167 per meg, respectively) (Surma et al., 2015; 2018; Herwartz et al., 2017). Plant water $\Delta'^{17}O$ values, which are highly sensitive to evaporation, range from –271 to +108 per meg (Fig. 1; Landais et al., 2006).

Similar to $\delta^{18}O_{enamel}$ values, $\Delta'^{17}O$ values of mammalian tooth enamel ($\Delta'^{17}O_{enamel}$) are influenced by the isotopic composition of food, drinking water, and atmospheric O_2 (Pack et al., 2013). The $\Delta'^{17}O$ value of O_2 is distinct and considerably lower than water with values that range between –432 ± 15 and −447 ± 34 per meg, based on recent compilations (Pack, 2021; Sharp and Wostbrock, 2021) (Fig. 1). In addition to the $\Delta'^{17}O$ value of O_2, relative humidity has a particularly strong influence on body water $\Delta'^{17}O$ values of mammalian herbivores, and hence $\Delta'^{17}O_{enamel}$ values, because it affects the degree of evaporation of ingested water (Passey and Levin, 2021).

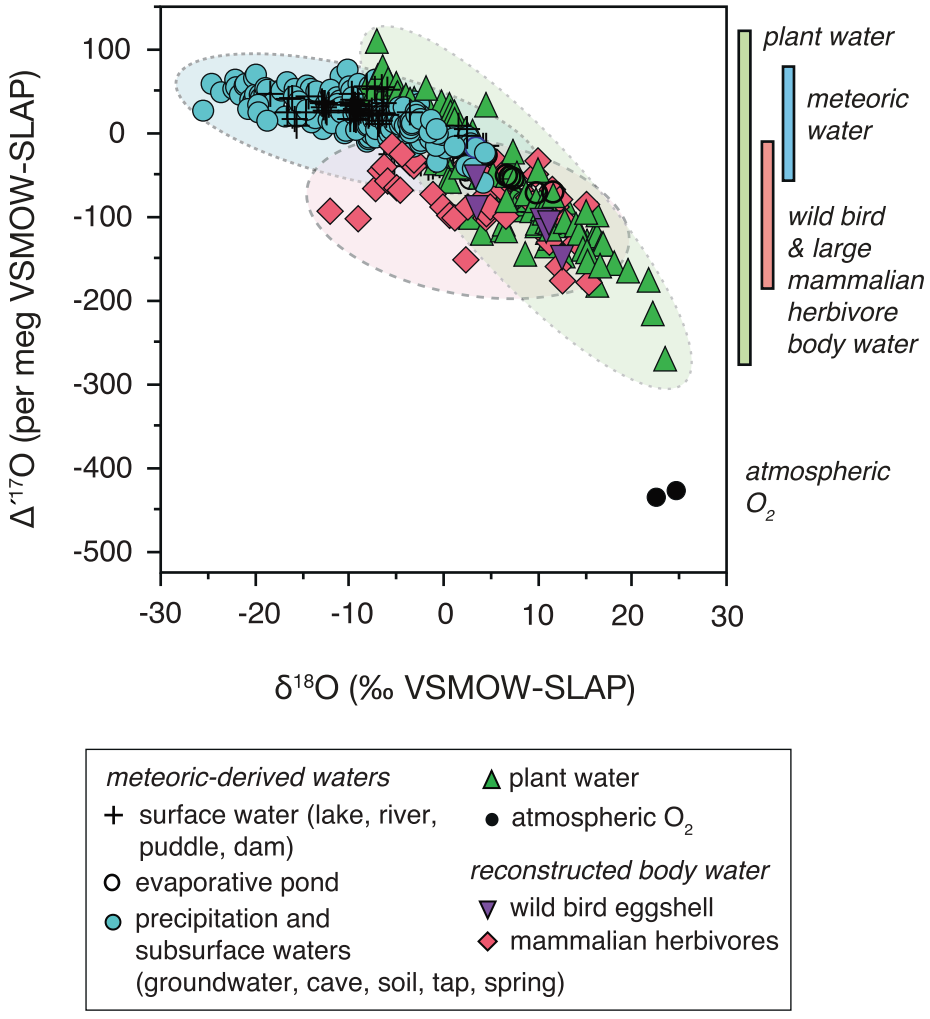

Fig. 1. $\Delta'^{17}O$ and $\delta^{18}O$ values of reconstructed body water for extant mammalian herbivores and birds and their primary input sources of oxygen: ingested plant water and drinking water, and inhaled atmospheric O_2. Body water $\Delta'^{17}O$ values are calculated from teeth and eggshells; see Section 4.1.2 for further discussion and references. Meteoric-derived waters are plotted for comparison. Vertical bars on right show the range of $\Delta'^{17}O$ values for sources of oxygen for mammals and their reconstructed body waters. Data are from Landais et al. (2006, 2010), Luz and Barkan (2010), Barkan and Luz (2011), Passey et al. (2014), Li et al. (2017), Surma et al. (2015; 2018), Herwartz et al. (2017), Passey and Ji (2019), Uechi and Uemura (2019), Whiteman et al. (2019), Pack et al. (2021), Sharp and Wostbrock (2021) and this study.

Please cite this article in press as: Lehmann S. B., et al. Triple oxygen isotope distribution in modern mammal teeth and potential geologic applications. *Geochim. Cosmochim. Acta* (2022), https://doi.org/10.1016/j.gca.2022.04.033

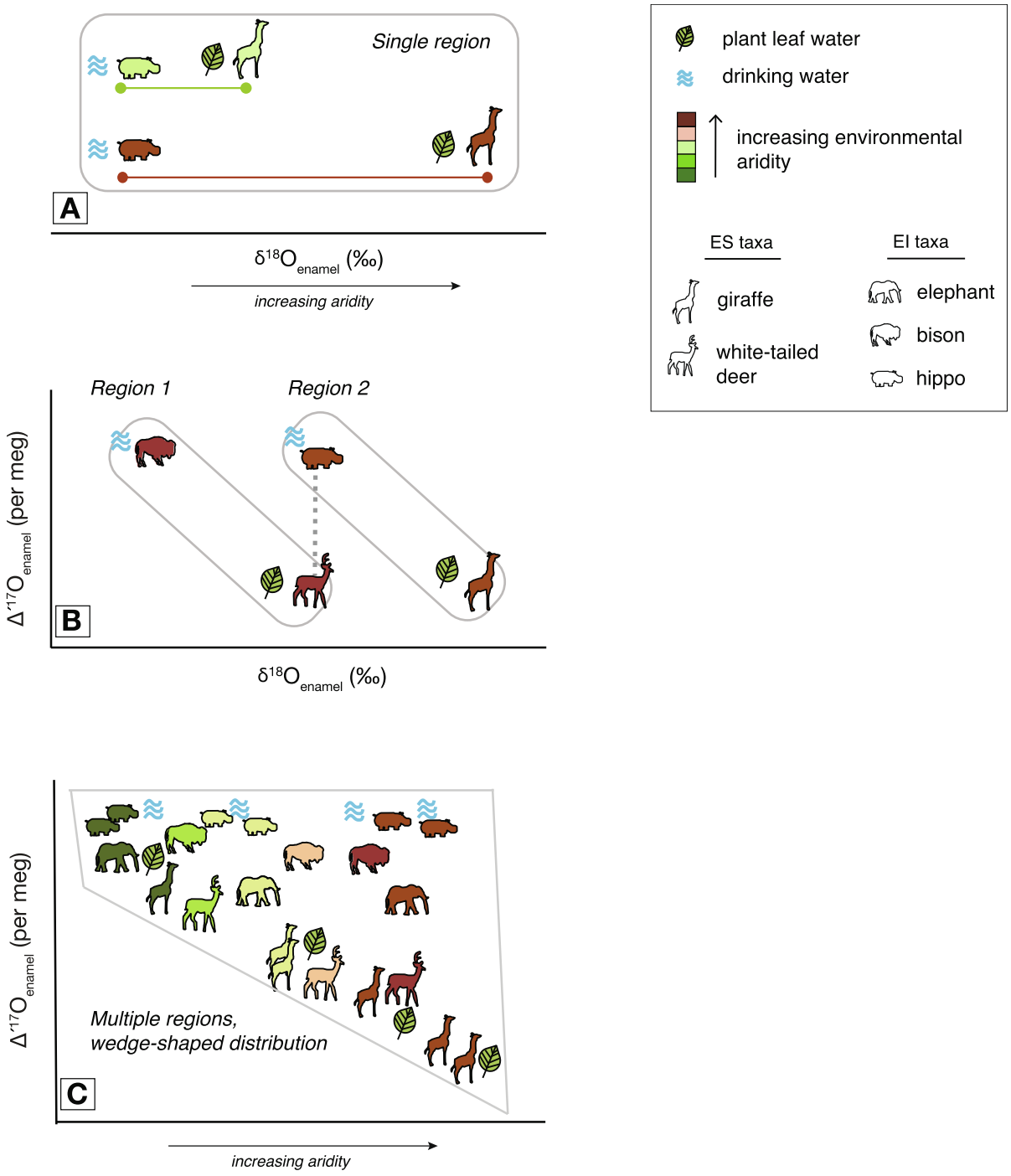

Fig. 2. Schematics outlining the variation of $\delta^{18}O_{enamel}$ and $\Delta'^{17}O_{enamel}$ values with aridity. A) The $\delta^{18}O_{enamel}$ value of evaporative-sensitive and evaporative-insensitive taxa from two environments within a single region where the $\delta^{18}O$ value of drinking water is constant. B) The $\delta^{18}O_{enamel}$ and $\Delta'^{17}O_{enamel}$ values of evaporative-sensitive (ES) and evaporative-insensitive (EI) taxa from environments with the same degree of aridity but from different regions, where $\delta^{18}O$ values of drinking water vary. Dashed gray line indicates how $\delta^{18}O_{enamel}$ values alone cannot distinguish a circumstance where aridity and input $\delta^{18}O$ values vary, whereas this distinction can be made with $\Delta'^{17}O_{enamel}$ values. C) Variation in $\Delta'^{17}O_{enamel}$ values vs. aridity for various locations and taxa spanning a range of behaviors and water-use strategies, showing a predicted wedge-shaped pattern.

Given the strong influence of evaporation on the oxygen isotopes of body water, we expect $\Delta'^{17}O_{enamel}$ values to vary with environment (Fig. 2B) such that they can be used as indicators of past aridity. Models of isotopic fractionation in body water suggest that animals who ingest the majority of their water from plants should have more negative

Please cite this article in press as: Lehmann S. B., et al. Triple oxygen isotope distribution in modern mammal teeth and potential geologic applications. *Geochim. Cosmochim. Acta* (2022), https://doi.org/10.1016/j.gca.2022.04.033

$\Delta'^{17}O_{enamel}$ values than animals that drink water regularly, due to evaporative enrichment of leaf water relative to surface waters (Passey and Levin, 2021; Fig. 2C). Given this, we predict that $\Delta'^{17}O_{enamel}$ values will exhibit more variance in arid environments, regardless of taxa and climatic features that vary according to geographic location of a site.

Here we present the $\Delta'^{17}O_{enamel}$ values of teeth from 50 extant herbivores from seven mammalian families and three continents to demonstrate variation in $\Delta'^{17}O_{enamel}$ values across different environments. We then outline approaches to using $\Delta'^{17}O_{enamel}$ records to reconstruct past aridity, in addition to its use in assessing post-depositional alteration of enamel oxygen isotopes and as a pCO_2 indicator.

2. MATERIALS AND METHODS

2.1. Site and sample selection

We designed our sample selection to evaluate the triple oxygen isotope distribution of teeth from large (>6 kg), extant mammalian herbivores that represented a range of water-use strategies and behaviors, continents, latitudes, and climates (Supplementary Table 1). We analyzed teeth from Hippopotamidae ($n = 4$), Elephantidae ($n = 9$), Bovidae ($n = 9$), Castoridae ($n = 2$), Cervidae ($n = 15$) and Giraffidae ($n = 6$). These data were combined with already published data from a Hippopotamidae, Bovidae, and Rhinocerotidae from Passey et al. (2014) and a Cervidae and Bovidae from Passey and Levin (2021). Teeth were collected over the past five decades and many samples have been used in previous studies (Cerling et al., 1999, 2004, 2008, 2015; Hoppe et al., 2006; Levin et al., 2008; Passey et al., 2014; Luyt et al., 2019; Passey and Levin, 2021). Specimens from Europe are from the Finnish Museum of National History.

2.2. Climate and aridity of sites

The geographic and climatic parameters for sites for which we report tooth enamel triple oxygen isotope data are listed in Table 1. We extracted mean annual temperature (MAT), precipitation (MAP), potential evapotranspiration (PET), percent relative humidity (rh), and Aridity Index (AI, where AI = MAP/PET) estimates for each location using the WorldClim Global Climate Data raster 1.4, or WorldClim1.4 (Hijmans et al., 2005; Trabucco and Zomer, 2009). We assigned corresponding UNESCO climate classifications to sites using AI data arid, semi-arid, subhumid, and humid, where UNESCO climate classifications are based on aridity indices and consider soil, vegetation, and topography (UNESCO, 1979). The $\delta^{18}O$ values of mean annual meteoric water were calculated using waterisotopes.org (Bowen and Revenaugh, 2003).

2.3. Sample preparation and analysis

For each tooth, enamel was removed along its growth axis, cleared of dentine and dirt, powdered, and homogenized. Powder was treated with 3% H_2O_2 to remove organic material, bathed in buffered acetic acid (0.1 *M*) to remove secondary carbonate, and dried at 60 °C. Analysis of triple oxygen isotopes of enamel (in this case the carbonate group of the bioapatite) followed the procedure outlined in Passey et al. (2014). We note that by analyzing carbonate group, we are only investigating a small portion (~5%) of the oxygen in enamel, as discussed in Bryant et al. (1996) and Xu et al. (2012). We refer to enamel throughout the text, but all results are from enamel carbonate.

Briefly, enamel powder (140–200 mg per analysis) was placed in silver capsules and reacted in a common bath of 100% phosphoric acid under vacuum at 90 °C to extract CO_2. CO_2 was then reduced to H_2O (Fe powder catalyst, 560 °C, 20 minutes), which was then fluorinated by passing through cobalt trifluoride at 370 °C, following methods described by Passey et al. (2014). The resultant O_2 was then analyzed by dual inlet isotope ratio mass spectroscopy on a Thermo Scientific MAT 253 at Johns Hopkins University. Samples were analyzed in duplicate or triplicate. We evaluated the stability of isotope measurements of external carbonate standards, both international (NBS18 and NBS19) and in–house (102–GC–AZ01) carbonates, and an inhouse CO_2 gas standard (Tank#2 CO_2). Water standards SLAP2 and VSMOW2 were directly injected into the cobalt trifluoride reactor to produce O_2 gas. The pooled standard deviation (1σ) for the external carbonate and CO_2 standards was 0.9‰ for $\delta^{18}O$ and 10 per meg for $\Delta'^{17}O$ over the time period when the samples were analyzed.

Carbonate oxygen isotope data were normalized to VSMOW2 ($\delta^{18}O = 0$‰ and $\delta^{17}O = 0$ per meg) and scaled to SLAP2 ($\delta^{18}O = -55.5$‰) using the reference frame $\Delta'^{17}O_{SLAP2} = 0$ per meg, where $\delta^{17}O_{SLAP2} = -29.6986$‰ when $\delta^{18}O_{SLAP2} = -55.5$‰ and $\lambda_{RL} = 0.528$ (Schoenemann et al., 2013). Using the recently proposed alternate value for $\Delta'^{17}O_{SLAP2}$ of −11 per meg (Wostbrock et al., 2020a) does not change the results that we report on carbonates. We normalize our $\Delta'^{17}O$ results to carbonate standards reported in Wostbrock et al. (2020a) so that they are comparable to $\Delta'^{17}O$ data of carbonates from other laboratories, as recommended by Sharp and Wostbrock (2021). To convert our measured $\Delta'^{17}O$ values of O_2 to $\Delta'^{17}O$ mineral (carbonate) we calculated the fractionation factors between the carbonate mineral and O_2 ($^{18}\alpha_{min\text{-}O2}$, $^{17}\alpha_{min\text{-}O2}$) for the acid digestion - fluorination - reduction procedure, using the $\delta^{18}O$ and $\Delta'^{17}O$ values of O_2 for the NBS19 standard that we measured during our study interval and comparing it to defined $\delta^{18}O$ and $\Delta'^{17}O$ values of the carbonate standard NBS19 ($\delta^{18}O = 28.65$‰, $\Delta'^{17}O = -102$ per meg) from Brand et al. (2014) and Wostbrock et al. (2020a), respectively. These calculated $\alpha_{min\text{-}O2}$ values account for fractionation in the 90 ℃ acid reaction, during the evolution of CO_2 and any other fractionation associated with our method. This approach assumes that the acid fractionation for enamel carbonate is the same as for calcite, which is necessary because there have not yet been studies that explore acid fractionation for enamel $\delta^{17}O$ values as has been done for $\delta^{18}O$ (e.g., Passey et al., 2007). After converting all data to the carbonate mineral equivalent values, using this universal approach, we then conducted a final correction for each analytical session based on the deviation of our

Please cite this article in press as: Lehmann S. B., et al. Triple oxygen isotope distribution in modern mammal teeth and potential geologic applications. *Geochim. Cosmochim. Acta* (2022), https://doi.org/10.1016/j.gca.2022.04.033

Table 1
Geographic, climatic and environmental information for sample locations.

Country	Location	Latitude	Longitude	Mean relative humidity (%) [a]	$\delta^{18}O$ MAP (‰ SMOW) [b]	*WorldClimWC 1.4 output* [c]					
						MAP (mm/yr)	MAT (°C)	PET (mm/yr)	Water deficit (mm/yr) [c]	Aridity Index	Aridity Index UNESCO category
Africa											
Kenya	Turkana	4.0	36.0	52.9	1.1	347	28	1897	1550	0.18	arid
Kenya	Meru National Park	0.1	38.2	63.2	1.7	512	24.5	2064	1552	0.24	semi-arid
Kenya	Shimba Hills National Park	−4.3	39.4	70.9	−3.5	1137	23.9	1493	356	0.75	semi-arid
Kenya	Laikipia/Mpala National Park	0.3	37.0	63.9	−0.8	713	18.2	1782	1069	0.39	semi-arid
Kenya	Tsavo National Park	−2.4	38.4	63.3	0.8	670	25	1836	1166	0.37	semi-arid
Kenya	Aberdares National Park	−0.4	36.7	70.2	−3.6	1780	10.1	1196	−584	1.52	humid
Ethiopia	Awash National Park	9.1	40.0	62.6	2.2	525	25.9	2091	1566	0.25	semi-arid
Uganda	Kidepo National Park	3.9	33.9	57.9	−1.1	614	22.9	1720	1106	0.34	semi-arid
DR Congo	Garamba National Park	4.2	29.5	67.1	0.2	1548	24.4	1813	265	0.86	humid
DR Congo	Ituri Forest National Park	1.4	28.6	71.6	−0.2	1739	24.4	1771	32	0.98	humid
South Africa	Kgalagadi National Park	−25.7	20.4	43.8	−4.7	230	20	1878	1648	0.12	arid
South Africa	Addo National Park	−33.5	25.7	64.2	−3.7	424	17.9	1398	974	0.32	semi-arid
Europe											
Finland	Noormarkku	61.6	21.9	81.6	−12.0	608	4	548	−60	1.11	humid
Finland/Sweden	Karessuando	68.4	22.5	86.5	−14.9	448	−2.2	393	−55	1.14	humid
Finland	Rovaniemi	66.5	25.7	80.0	−13.1	513	0.4	458	−55	1.13	humid
Finland	Pernaja	60.4	26.1	81.1	−11.8	618	4.7	547	−71	1.13	humid
Karelia, Russia	Aunus Nurmoila	61.1	32.9	81.8	−12.0	672	2.9	541	−131	1.24	humid
North America											
United States	Badlands National Park, SD	43.9	−102.3	60.5	−9.9	415	8.6	1109	694	0.37	semi-arid
United States	Theodore Roosevelt National Park, ND	47.0	−103.5	63.9	−11.4	383	6.3	982	599	0.40	semi-arid
United States	Wichita Mountains Federal Wildlife Refuge, OK	34.7	−98.7	63.7	−5.8	735	15.4	1358	623	0.54	subhumid
United States	Antelope Island, UT	41.0	−112.2	54.3	−14.1	462	10.1	1026	564	0.57	subhumid
United States	Parowan, UT	37.8	−112.8	48.1	−12.7	320	8.9	1229	909	0.26	semi-arid
United States	Arctic National Wildlife Refuge, AK	68.6	−142.9	67.9	−26.0	154	−13.9	263	109	0.58	subhumid
United States	Middle Fork, Selman River, ID	44.9	−115.0	59.9	−16.6	581	−0.1	789	208	0.74	subhumid
United States	Piedmont National Wildlife Refuge, GA	33.1	−83.7	70.2	−5.5	1213	17.3	1415	202	0.86	humid
United States	Berkley Springs, WV	39.6	−78.2	69.6	−8.2	949	10.7	1093	144	0.87	humid
United States	Baltimore, MD	39.3	−76.6	66.6	−6.7	1110	12.9	1142	32	0.96	humid
United States	Westchester County, NY	41.1	−73.8	67.7	−7.6	1227	10.6	980	−247	1.26	humid
United States	Dairymens Country Club, WI	46.1	−89.7	72.6	−10.8	834	3.8	819	−15	1.02	humid
United States	Yellowstone National Park, WY	44.4	−110.6	55.7	−16.8	646	−1	760	114	0.82	humid
United States	Edness Kimball Wilkins State National Park, WY	42.9	−106.2	55.3	−13.0	311	7.9	1105	794	0.28	semi-arid

[a] CRU 2.0 output dataset for mean relative humidity (New et al., 2002).
[b] The Online Isotopes in Precipitation Calculator data for mean annual precipitation (version 3.1, https://www.waterisotopes.org) (Bowen and Revenaugh, 2003).
[c] Mean annual precipitation (MAP), mean potential evapotranspiration (PET), Water deficit is PET - MAP.

Please cite this article in press as: Lehmann S. B., et al. Triple oxygen isotope distribution in modern mammal teeth and potential geologic applications. *Geochim. Cosmochim. Acta* (2022), https://doi.org/10.1016/j.gca.2022.04.033

measured $\Delta'^{17}O_{carbonate}$ values of NBS19 to those reported by Wostbrock et al. (2020a). Furthermore, we used analyses of other carbonate and CO_2 reference materials (e.g., NBS18, 102-GC-AZ01, Tank #2 CO_2) to evaluate these corrections (Table S2) and we observe that the relative $\Delta'^{17}O$ values of these materials is consistent, within error, across our analytical sessions and with the spacing of $\Delta'^{17}O$ values among these materials observed in other studies (e.g. Passey et al., 2014; Wostbrock et al., 2020a; Passey and Levin, 2021). All data for standards are reported in Supplementary Table 2, which will allow for subsequent renormalization of our dataset when the necessary fractionation factors are determined.

All data from analytical sessions are reported in Supplementary Table 3. Data were evaluated using the statistical analytical software JMP 11 produced by the SAS Institute. Oxygen isotope measurements are described using $\Delta'^{17}O$ and $\delta^{18}O$ notation, δ-values are reported in per mil (‰) relative to VSMOW, and $\Delta'^{17}O$ values are reported in per meg, where 1‰ is 1000 per meg and defined with a reference slope of 0.528. As with carbonate standards, we report the oxygen isotope data from tooth enamel samples in the mineral form. Throughout the text the ± symbol indicates one standard deviation from the mean and data are reported as mean ± 1σ. For reporting analytical error associated with replicate analyses of the same sample, we represent the error using the 1σ when n > 2 analyses and absolute difference between pairs of analyses (n = 2). We recognize that these measures do not provide a true representation of the uncertainty on the mean and that the true error could be larger.

We used pairwise analyses to evaluate isotopic differences between latitudes, families, and climate categories. However, while our $\delta^{18}O_{enamel}$ data are normally distributed, our $\Delta'^{17}O_{enamel}$ data deviate from normality as shown in Supplementary Fig. 1. Due to these differences, we use parametric ANOVA tests to evaluate $\delta^{18}O_{enamel}$ and nonparametric Wilcoxon and Kruskal-Wallis tests to evaluate distinctions in $\Delta'^{17}O_{enamel}$ values. Differences among-groups were evaluated using Tukey-Kramer HSD and the Steel-Dwass method. To test for differences in variance, we used the parametric Bartlett's test and nonparametric Levene's test for $\delta^{18}O_{enamel}$ and $\Delta'^{17}O_{enamel}$, respectively. Within each family, we used linear regression to evaluate the relationship between changes in aridity and associated changes in isotope values. Because samples from the same region share the same aridity index, it is necessary to account for this non-independence among the data prior to analysis. To do this, all isotope values from each site are first summarized as the median of those values before evaluating the linear regression.

3. RESULTS

3.1. Variation by latitude and region

Among all the herbivores, $\Delta'^{17}O_{enamel}$ values range from −252 to −90 per meg (−149 ± 38 per meg) and $\delta^{18}O_{enamel}$ values range from 17.0‰ to 40.2‰ (29.1 ± 6.5‰) (Table 2; Fig. 3). $\Delta'^{17}O_{enamel}$ values do not correlate with absolute latitude ($R^2 = 0.0266$, $p = 0.2961$; Fig. 3B). $\delta^{18}O_{enamel}$ values decrease with increasing absolute latitude ($R^2 = 0.6321$, $p < 0.0001$), such that teeth sampled from low latitudes (0 – 24°, $n = 23$) yield $\delta^{18}O_{enamel}$ values that are significantly different ($p < 0.0001$) than those from mid latitudes (24 – 66°, $n = 24$) (Fig. 3A). The lack of obvious differences in the $\delta^{18}O_{enamel}$ values from mid and high latitudes may be an artifact of limited samples from high latitudes (>66°, $n = 3$).

3.2. Variation by aridity

Our sampled teeth come from a range of environments with a broad range of Aridity Index (AI) values: 0.12 to 1.52 (Table 1). UNESCO climate classifications of these environments, informed by our AI data, are humid (AI > 0.75, $n = 22$), subhumid (AI 0.5–0.75, $n = 3$), semi–arid (AI 0.2–0.5, $n = 16$), and arid (AI < 0.2, $n = 9$) (UNESCO, 1979). Environments include the arid Turkana and Kgalagadi regions in Africa (AI = 0.18 and 0.12, respectively), mid latitude semi–arid Utah (AI = 0.26), high latitude, cold, subhumid Alaska (AI = 0.58), moist Kenyan highlands (AI = 1.51), and cool, humid Finland (AI > 1.01).

The distribution of $\Delta'^{17}O_{enamel}$ values form a wedge–shaped pattern when plotted against AI (Fig. 3B, E). We also find that the variances of $\Delta'^{17}O_{enamel}$ values from arid and semi-arid sites ($n = 25$, −252 to −90 per meg, −161 ± 45 per meg) have statistically different variance from subhumid and humid sites ($n = 25$, −178 to −102 per meg, −138 ± 26 per meg) (df = 1, F = 5.6083, $p = 0.0220$). The $\delta^{18}O_{enamel}$ values from more arid sites (17.5 to 40.2‰, 31.8 ± 6.2‰) are not different from $\delta^{18}O_{enamel}$ values from more mesic sites (17.0 to 39.9‰, 26.5 ± 5.7‰) (df = 1, F = 0.1372, $p = 0.7111$).

3.3. Variation by taxon

We observe that herbivore $\Delta'^{17}O_{enamel}$ and $\delta^{18}O_{enamel}$ values can vary by taxonomy (Table 2; Supplementary Table 4; Fig. 3 D – F).

In Africa, our sample includes giraffids ($n = 7$), bovids ($n = 5$), a rhinocerotid ($n = 1$), elephantids ($n = 9$) and hippopotamids ($n = 5$) from South Africa, Kenya, Uganda, and the Democratic Republic of the Congo. The $\Delta'^{17}O_{enamel}$ values of hippopotamids are significantly higher than those of giraffids ($p = 0.0456$). Pooled together, the $\Delta'^{17}O_{enamel}$ values of hippopotamids are not distinct from elephantids ($p = 0.1558$), though within each environment, hippopotamid values are consistently higher. Giraffid and bovid $\Delta'^{17}O_{enamel}$ values generally overlap ($p = 0.9886$) and show large ranges in $\Delta'^{17}O_{enamel}$ (>100 per meg). In our taxonomic divisions, giraffids include samples of giraffe and okapi while the bovids include samples from buffalo, wildebeest, oryx and hartebeest. Giraffid and bovid $\Delta'^{17}O_{enamel}$ values are negatively correlated with AI (bovids, $R^2 = 0.7823$, $p = 0.0295$; giraffids, $R^2 = 0.8695$, $p = 0.0042$). The $\Delta'^{17}O_{enamel}$ values for elephantids and hippopotamids exhibit a narrow range across AI (<45 per meg) and have

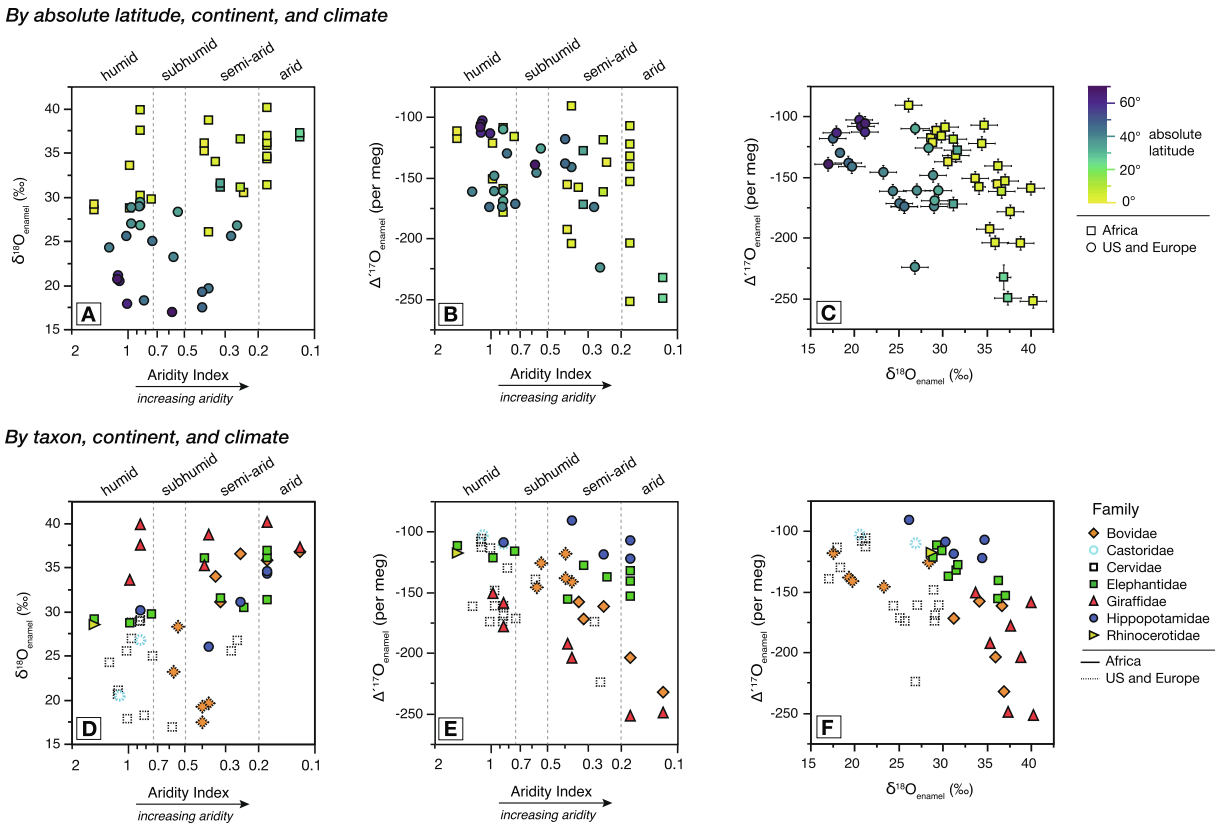

Fig. 3. Distribution of $\delta^{18}O_{enamel}$ and $\Delta'^{17}O_{enamel}$ values by latitude, location, taxon, and climate. In plots A – C, the geography of sample site is indicated using a color gradient for absolute latitude and symbols according to region. In plots D – F, taxa are grouped by family. Aridity Index is presented on a log scale and corresponding UNESCO climate categories are separated by vertical dashed lines. In plot C, error bars are plotted as 1σ on the mean for samples with $n > 2$ analyses. For the error bars associated with samples for which there are only duplicate analyses ($n = 44$), we use the absolute differences between pairs of analyses. Given the small number of replicates for all samples we recognize that these errors do not provide a true representation of the uncertainty on the mean and that the true error could be larger.

$R^2 = 0.4795$ ($p = 0.0510$) and $R^2 = -0.4428$ ($p = 0.8047$), respectively. The distribution of $\delta^{18}O_{enamel}$ values of the different taxa mostly overlap with one another. Taxonomic families showed no evidence for significant correlations between $\delta^{18}O_{enamel}$ values and AI: $R^2 = -0.3587$ ($p = 0.6930$) for hippopotamids, $R^2 = 0.3144$ ($p = 0.1105$) for elephantids, $R^2 = 0.4174$ ($p = 0.1440$) for bovids, and $R^2 = 0.0468$ ($p = 0.3270$) for giraffids.

The samples from North America and Europe include teeth from bovids ($n = 5$), castorids ($n = 2$) and cervids ($n = 16$). The $\Delta'^{17}O_{enamel}$ values of castorids and bovids represent a tighter range (–146 to –102 per meg, –126 ± 16 per meg) than that of cervids (–224 to –105 per meg, –151 ± 32 per meg). In comparison, the ranges of cervid and bovid $\delta^{18}O_{enamel}$ values are similar across AI (mean difference = 2.574148, $p = 0.4806$). Castorids from humid environments and their $\delta^{18}O_{enamel}$ values overlap with those of cervids and bovids from humid to semi-arid environments.

Although not visible on Fig. 3, where taxa are grouped by family, it is important to note that three species of cervids were sampled (moose (*Alces alces*) $n = 3$, reindeer/caribou (*Rangifer tarandus sps.*) $n = 3$, and white-tailed deer (*Odocoileus virginia*) $n = 10$) spanning humid to semi-arid environments. White-tailed deer yield lower $\Delta'^{17}O_{enamel}$ values than those of moose and reindeer/caribou. There is no equivalent distinction in $\delta^{18}O_{enamel}$ values.

4. DISCUSSION

4.1. Variation of $\Delta'^{17}O_{enamel}$ values

4.1.1. Observations

The $\Delta'^{17}O_{enamel}$ values from extant herbivores from Africa, Europe and North America can vary by 145 per meg (–252 to –107 per meg) at sites with data from multiple taxa. In comparison, the $\Delta'^{17}O$ values of plant waters span up to 189 per meg in a single environment (Li et al., 2017) and are sensitive to variation in relative humidity between environments (Alexandre et al., 2018), while the $\Delta'^{17}O$ values of meteoric waters across all environments span 85 per meg (Landais et al., 2006, 2010; Luz and Barkan, 2010; Passey et al., 2014; Li et al., 2017; Passey and Ji, 2019).

The combined influences of aridity and animal water-use strategy seem to be the strongest determinants of $\Delta'^{17}O_{enamel}$ values across the geographic and environmental gradients that we sampled. We observe a greater variation in $\Delta'^{17}O$ in arid and semi-arid environments, than in humid

Please cite this article in press as: Lehmann S. B., et al. Triple oxygen isotope distribution in modern mammal teeth and potential geologic applications. *Geochim. Cosmochim. Acta* (2022), https://doi.org/10.1016/j.gca.2022.04.033

Table 2
Compilation of oxygen isotope data for tooth enamel specimens and calculated body waters.

			Corrected mean enamel oxygen isotopic values[a]								*Calculated $\Delta'^{17}O$ body water values*[d]		
Analytical ID (first # of a series)	**Sample ID**	**Common name**	**$\delta^{17}O$ (‰)**	**±**[b]	**$\delta^{18}O$ (‰)**	**±**[b]	**$\Delta'^{17}O$ (‰)**	**$\Delta'^{17}O$ (per meg)**	**±**[b]	***n***[c]	**$\delta^{18}O$ (‰)**	**$\Delta'^{17}O$ (‰)**	**$\Delta'^{17}O$ (per meg)**
Africa													
JHU-17O-2326	Kidepo buffalo	African buffalo	17.68	0.40	34.06	0.70	−0.157	−157	6.21	4	9.43	−0.085	−85
JHU-17O-2331	UCT 14224 Kalagadi Wildebeest	Blue wildebeest	19.06	0.40	36.86	0.80	−0.232	–232	10.21	3	12.16	−0.160	−160
JHU-17O-2057	TMO (TRK05-103-ORX)	Oryx	18.58	0.23	35.89	0.43	−0.203	−203	5.46	2	11.22	−0.131	−131
JHU-17O-2160	ET05-AWSH-04	Oryx	19.01	0.34	36.62	0.66	−0.161	−161	3.55	2	11.93	−0.089	−89
JHU-17O-2341	UCT 14285 Addo hartebeest	Red/Cape hartebeest	16.16	1.15	31.16	2.23	−0.172	−172	12.51	2	6.60	−0.100	−100
JHU-17O-2059	ET05-MAGO-19	Elephant	19.22	0.03	37.00	0.06	−0.153	−153	7.06	2	12.30	−0.080	−80
JHU-17O-2154	ET05-MAG0-10 elephant	Elephant	18.82	0.37	36.21	0.72	−0.140	−140	1.87	2	11.53	−0.068	−68
JHU-17O-2156	MGL-93-06	Elephant	16.34	0.20	31.43	0.37	−0.132	−132	3.26	2	6.86	−0.059	−59
JHU-17O-2320	MGL-93-17 Meru elephant	Elephant	15.87	0.68	30.55	1.33	−0.137	−137	11.26	2	6.00	−0.065	−65
JHU-17O-2322	MGL-93-10 Shimba Hills elephant	Elephant	15.51	0.30	29.81	0.59	−0.116	−116	11.35	2	5.28	−0.043	−43
JHU-17O-2079	MGL-93-16	Elephant	18.77	-	36.16	-	−0.155	−155	-	1	11.48	−0.083	−83
JHU-17O-2052	CME (MF-F-5)	Elephant	14.98	0.20	28.81	0.50	−0.121	−121	2.09	3	4.30	−0.049	−49
JHU-17O-2315	MGL-93-7 Aberdares elephant	Elephant	15.22	0.30	29.23	0.58	−0.111	−111	2.50	2	4.72	−0.039	−39
JHU-17O-2324	UCT 1697 Addo elephant	Elephant	16.44	0.38	31.62	0.74	−0.127	−127	2.40	2	7.05	−0.055	−55
JHU-17O-2055	KN07-108	Giraffe	20.76	0.15	40.19	0.28	−0.252	−252	3.85	2	15.41	−0.179	−179
JHU-17O-2077	K00-TSV-113	Giraffe	20.07	0.05	38.76	0.09	−0.204	−204	3.26	2	14.02	−0.131	−131
JHU-17O-2071	GNP-giraffe2	Giraffe	19.5	0.52	37.60	1.00	−0.178	−178	3.90	2	12.89	−0.106	−106
JHU-17O-2300	GNP giraffe #1	Giraffe	20.72	1.10	39.92	2.15	−0.159	−159	16.15	2	15.15	−0.086	−86
JHU-17O-2075	K98-Lai-310	Giraffe	18.28	0.50	35.28	0.98	−0.192	−192	12.73	2	10.62	−0.120	−120
JHU-17O-2339	UCT 14223 Kgalagadi giraffe#1	Giraffe	19.28	1.57	37.32	3.05	−0.249	−249	13.62	2	12.61	−0.177	−177
JHU-17O-2073	Ituri Giraffe	Okapi	17.46	0.11	33.63	0.22	−0.151	−151	1.06	2	9.01	−0.078	−78
JHU-17O-2158	KN07-111	Hippo	18.04	0.03	34.65	0.07	−0.107	−107	4.74	2	10.01	−0.034	−34
JHU-17O-2048	KN07-112	Hippo	17.88	0.26	34.38	0.48	−0.122	−122	7.70	2	9.74	−0.050	−50
JHU-17O-2151	ET05-AWSH-29 (HIPPO)	Hippo	16.21	0.02	31.16	0.04	−0.118	−118	1.89	2	6.60	−0.046	−46
JHU-17O-1147	K00-TSV-226	Hippo	13.6	0.04	26.10	0.07	−0.090	−90.4	5.90	2	1.66	−0.018	−18
JHU-17O-2069, -1148	GNP-Hippo	Hippo	15.73	0.05	30.22	0.07	−0.108	−108	12.46	2	5.68	−0.036	−36
JHU-17O-1149, -1150	K00-AB-303p4	Black rhino	14.88	0.32	28.61	0.60	−0.117	−117	5.27	2	4.11	−0.045	−45
Europe													
JHU-17O-2486	CF2/ KN 6751/ Finland Beaver#2	Beaver	10.68	0.83	20.53	1.60	−0.102	−102	2.14	2	−3.78	−0.030	−30
JHU-17O-2482	FT1/ UN 2319/ Finland Deer#1	Reindeer	10.78	0.77	20.73	1.49	−0.108	−108	10.02	2	−3.58	−0.036	−36
JHU-17O-2484	RT1/ KN 1494/ Finland Deer#3	Reindeer	11.02	0.28	21.18	0.53	−0.105	−105	1.83	2	−3.14	−0.033	–33
JHU-17O-2480	AA1/ KN 46564/ Finland Moose #1	Moose	11.01	0.59	21.17	1.11	−0.112	−112	4.66	2	−3.16	−0.040	−40
JHU-17O-2488	AA2/ KN 49036/ Finland Moose#2	Moose	9.321	0.32	17.95	0.60	−0.113	−113	5.96	2	−6.30	−0.041	−41
North America													
JHU-17O-2556	SD bison #1	Bison	10.21	0.64	19.69	1.20	−0.141	−141	8.94	2	−4.60	−0.069	−69
JHU-17O-2542	OK Bison #1	Bison	14.75	0.97	28.36	1.87	−0.126	−126	0.71	2	3.86	−0.054	−54
JHU-17O-2552	ND bison #1	Bison	9.10	0.65	17.54	1.28	−0.118	−118	17.92	2	−6.70	−0.046	−46
JHU-17O-2554	ND bison #2	Bison	10.00	0.42	19.30	0.80	−0.138	−138	2.74	2	−4.98	−0.066	−66

JHU-17O-2080	AIJB-B3-T4-DP4	Bison	12.06	0.65	23.25	1.26	−0.146	−146	3.23	2	−1.13	−0.074	−74
JHU-17O-2328	GA Beaver	Beaver	13.97	0.8	26.84	1.6	−0.110	−110	4.844	4	2.39	−0.038	−38
JHU-17O-2539	AK Caribou #1	Caribou	8.81	0.76	17.01	1.46	−0.139	−139	0.60	2	−7.21	−0.067	−67
JHU-17O-2541	WY Yellowstone Moose #1	Moose	9.50	-	18.32	-	−0.130	−130	-	1	−5.93	−0.058	−58
JHU-17O-2537	WY deer	White-tailed deer	13.27	0.54	25.62	1.04	−0.174	−174	4.48	2	1.19	−0.102	−102
JHU-17O-2061	UT-deer	White-tailed deer	13.84	0.01	26.81	0.00	−0.224	−224	11.59	2	2.36	−0.152	−152
JHU-17O-2535	ID deer	White-tailed deer	12.98	0.95	25.06	1.85	−0.171	−171	16.87	2	0.64	−0.099	−99
JHU-17O-2347	GA deer 1	White-tailed deer	15.29	0.31	29.46	0.58	−0.161	−161	8.33	2	4.94	−0.089	−89
JHU-17O-2343	GA deer 2	White-tailed deer	15.06	0.43	29.05	0.81	−0.169	−169	2.80	2	4.54	−0.097	−97
JHU-17O-2524	WV deer	White-tailed deer	15.02	0.35	28.98	0.66	−0.174	−174	2.72	2	4.47	−0.102	−102
JHU-17O-2520	MD deer #1	White-tailed deer	14.99	0.78	28.87	1.51	−0.148	−148	6.25	2	4.36	−0.076	−76
JHU-17O-2522	MD deer #2	White-tailed deer	14.02	0.41	27.04	0.79	−0.161	−161	1.50	2	2.57	−0.089	−89
JHU-17O-2345	NY deer 1	White-tailed deer	12.61	0.11	24.32	0.23	−0.161	−161	7.53	2	−0.07	−0.089	−89
JHU-17O-2526	WI deer	White-tailed deer	13.27	0.51	25.62	1.00	−0.174	−174	9.99	2	1.19	−0.102	−102

[a] $\delta^{18}O$, $\delta^{17}O$ and $\Delta'^{17}O$ values normalized to VSMOW-SLAP scale, as per Schoenemann et al. (2013) with $\lambda = 0.528$ and normalized to known $\delta^{18}O(CO_2/mineral)$ values, as described in the Methods Section.

[b] Errors are represented as 1σ when $n > 2$ analyses and absolute difference between pairs of analyses ($n = 2$). Values are ‰ for $\delta^{17}O$ and $\delta^{18}O$ and per meg for $\Delta'^{17}O$. The absolute differences between pairs of analyses are used in the calculation of error plotted in Fig. 3C for samples where $n = 2$.

[c] Number of analyses, where each analysis involves extraction of CO_2 from enamel carbonate, reduction and fluorination of CO_2 to O_2, and analysis on a Thermo MAT 253 mass spectrometer.

[d] Body water triple oxygen isotope values are calculated using the relationship $^{17}\alpha_{enamel\text{-}body\ water} = (^{17}\alpha_{enamel\text{-}body\ water})^{\theta}$. See Section 4.1.2 in text for discussion and references.

environments, resulting in a wedge-shaped pattern in a plot of AI vs. $\Delta'^{17}O_{enamel}$ that persists across a range of latitudes and $\delta^{18}O$ values of meteoric water (Fig. 3B). This relationship is not found between $\delta^{18}O_{enamel}$ and aridity (Fig. 3A). Instead, $\delta^{18}O_{enamel}$ more closely tracks latitude, reflecting the well-known correlation between $\delta^{18}O$ values of meteoric water and latitude (e.g., Dansgaard, 1964).

The wedge-shaped $\Delta'^{17}O_{enamel}$ – aridity relationship is, in part, driven by variability in water-use strategies of our sampled taxa. As discussed above, water-use strategy is influenced by diet, physiology, and behavior. An important factor in water-use strategy is animal's water dependence, which can be characterized by the Water Economy Index, where Water Economy Index = ml H_2O ingested per kJ of metabolic energy (see Nagy and Peterson, 1988). Animals with low Water Economy Index values are less dependent on surface waters and can more readily sustain water requirements based on dietary water (leaf water, root/stem water, metabolic water; Kohn, 1996). Oxygen isotope distributions in animals generally group into two categories, evaporation-sensitive and evaporation-insensitive, where $\delta^{18}O_{enamel}$ values of evaporation-insensitive taxa (high Water Economy Index) do not vary with aridity and $\delta^{18}O_{enamel}$ values of evaporation-sensitive taxa (low Water Economy Index) increase with aridity (Levin et al., 2006; Blumenthal et al., 2017). We classify taxa as evaporation-sensitive or evaporation-insensitive using previously published work when possible and otherwise assign a suggested evaporation-sensitive or evaporation-insensitive classification based on an animal's water and food intake (Table 3).

When $\Delta'^{17}O_{enamel}$ data from the entire dataset are pooled and taxa are grouped by the two water-use categories, $\Delta'^{17}O_{enamel}$ values of evaporation-sensitive taxa are both lower and slightly more varied than those of evaporation-insensitive taxa (Fig. 4A). Evaporation-sensitive taxa yield $\Delta'^{17}O_{enamel}$ values with a 104 per meg range (−252 to −148 per meg) whereas $\Delta'^{17}O_{enamel}$ values of evaporation-insensitive taxa have a 65 per meg range (−155 to −90 per meg). The distinctions in $\Delta'^{17}O_{enamel}$ values between evaporation-sensitive and evaporation-insensitive taxa persist across the three continents and different climate regimes. In contrast, $\delta^{18}O_{enamel}$ values of evaporation-sensitive and evaporation-insensitive taxa are not distinct, in part because they are strongly influenced by local meteoric water $\delta^{18}O$ values which exert a stronger influence on $\delta^{18}O_{enamel}$ values than animal water-use strategies (Fig. 4B). The clear distinctions in $\Delta'^{17}O_{enamel}$ values between evaporation-sensitive and evaporation-insensitive taxa show the importance of including samples from taxa with a range of water-use strategies to assess the distribution of $\Delta'^{17}O_{enamel}$ values from any location.

4.1.2. $\Delta'^{17}O_{enamel}$ values in light of the $\Delta'^{17}O$ body water model

Accurate isotope mass-balance body water models are critical for understanding the controls on oxygen isotopic variation in tooth enamel. Of the body water models developed for $\delta^{18}O$, some are scaled to body mass and metabolic rate (e.g., Bryant and Froelich, 1995), whereas others consider animal behavior and physiology which can influence

Table 3
Animal behavior summary for reported taxa.

Common name	Family	Genus and species	Diet	General water use strategy	ES or EI status[a]
Red/Cape hartebeest	Bovidae	*Alcelaphus buselaphus caama*	Grazer	[e, i]Not very water dependent	-
Bison	Bovidae	*Bison bison bison*	Grazer	[h]Water dependent	EI
Blue wildebeest	Bovidae	*Connochaetes taurinus taurinus*	Grazer	[i]Not very water dependent	-
Oryx	Bovidae	*Oryx gazella beisa*	Grazer	[b, e, i]Not water dependent	ES
African buffalo	Bovidae	*Syncerus caffer*	Grazer	[e, i]Water dependent	-
Beaver	Castoridae	*Castor fiber*	Semi-aquatic	[d]Water dependent	EI
Moose	Cervidae	*Alces alces*	Mixed feeder/Semi-aquatic	[d]Water dependent	EI
White-tailed deer	Cervidae	*Odocoileus virginianus virginianus*	Mixed feeder	[c]Not water dependent	ES
Reindeer and Caribou	Cervidae	*Rangifer tarandus*	Browser/Mixed feeder	[d]Not very water dependent	-
Elephant	Elephantidae	*Loxodonta africana africana*	Browser	[i]Water dependent	EI
Giraffe	Giraffidae	*Giraffa camelopardalis*	Browser	[g, i]Not water dependent	ES
Okapi	Giraffidae	*Okapia johnstoni*	Browser	[f, g, i]Not water dependent	ES
Hippo	Hippopotamidae	*Hippopotamus amphibius amphibius*	Semi-aquatic	[g, i]Water dependent	EI
Black rhino	Rhinocerotidae	*Diceros bicornis*	Browser/Grazer	[i]Water dependent	EI

[a]Data are classified as evaporation sensitive (ES) or evaporation insensitive (EI) based on the relationship between $\delta^{18}O$ values and aridity and relative humidity based on previously published work. For taxa that have not been classified as ES and EI, we evaluated their diet, water use, and Water Economy Index when available to suggest ES or EI classification.
References ([b]Kohn et al., 1996; [c]Luz et al., 1990; [d]Nowak, 1999; [e,f]Cerling et al., 2003, 2004; [g]Levin et al., 2006; [h]Hoppe et al., 2006; [i]Blumenthal et al., 2017).

$\delta^{18}O$ independently of animal mass (e.g., Kohn, 1996). The latter is effective at predicting $\delta^{18}O_{enamel}$ across aridity gradients (e.g., Blumenthal et al., 2017) because it accounts for variation in fluxes of water that undergo evaporation, including both water that is consumed (e.g., leaf waters, surface waters) and released by an animal (e.g., vapor loss during breathing, panting).

With increased interest in triple oxygen isotopes, isotope mass-balance body water models have been adapted to consider $\Delta'^{17}O$, using approaches that either scale to animal mass (Pack et al., 2013; Whiteman et al., 2019) or link to animal physiology and behavior (Passey and Levin, 2021). While some studies demonstrate positive trends between $\Delta'^{17}O$ values of body water ($\Delta'^{17}O_{body\ water}$) and body mass (Pack et al., 2013; Whiteman et al., 2019), there is considerable scatter in $\Delta'^{17}O_{body\ water}$ values (>200 per meg) among animals that do not vary in body mass but that do vary in Water Economy Index (Passey and Levin, 2021). This latter observation indicates the importance of physiology, behavior, and environment in determining $\Delta'^{17}O$ values in animals, as has been observed for $\delta^{18}O$ (e.g., Luz et al., 1990; Levin et al., 2006; Blumenthal et al., 2017).

Here we compare the $\Delta'^{17}O_{enamel}$ results from this study to outputs from an isotope mass-balance model to understand why $\Delta'^{17}O_{enamel}$ values vary among different taxa and across environmental gradients. We use a modeling approach that allows for the adjustment of fluxes of oxygen in and out of animals based on a version of the Kohn (1996) model that is modified for triple oxygen isotopes (Passey and Levin, 2021). We modeled animal physiology and behavior considering four different scenarios: 1) a standard evaporation-sensitive condition where an animal is efficient with its water use (low Water Economy Index), has dry feces and consumes a large relative fraction of leaf water (e.g., giraffe, deer); 2) a water-dependent animal with high Water Economy Index, wet feces, but with a low proportion of consumed leaf water (e.g., hippos, beaver); 3) another water-dependent condition where an animal has a high Water Economy Index and wet feces, but consumes a high proportion of leaf water (e.g., elephant); and 4) an evaporation-sensitive condition where an animal has low Water Economy Index and dry feces but consumes very little leaf water (e.g., reindeer, caribou). These four scenarios are represented by the four different lines in Fig. 5. Model conditions used for these scenarios are presented in Supplementary Tables 5 and 6. In selecting the conditions for these different scenarios, we focused on varying Water Economy Index, fecal water, sweating, food quality (digestibility) and food water content because these parameters are established metrics for tracking variation the fluxes of oxygen through an animal in varying environmental conditions. While variations in metabolic rates affect the absolute rate of O_2 intake, they do not change the relative intake of atmospheric O_2 compared to other oxygen sources (e.g., food water, drinking water; see Passey and Levin (2021) for a more detailed discussion). We use relative humidity to represent environmental variation as it is a physical parameter that controls oxygen isotope fractionation, in contrast to using the Aridity Index or water deficit terms which are used

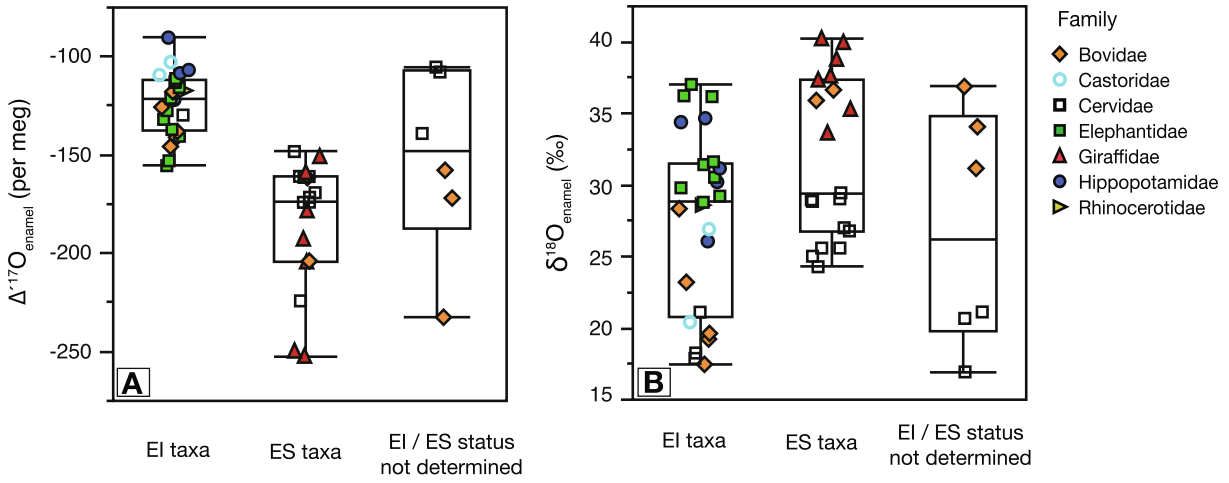

Fig. 4. Box plots of A) $\Delta'^{17}O_{enamel}$ and B) $\delta^{18}O_{enamel}$ values of taxa grouped by the of evaporation insensitive (EI) and evaporation sensitive (ES) classification and plotted by family. Box ends are the quartile values, inner horizontal line the median, and whiskers the range.

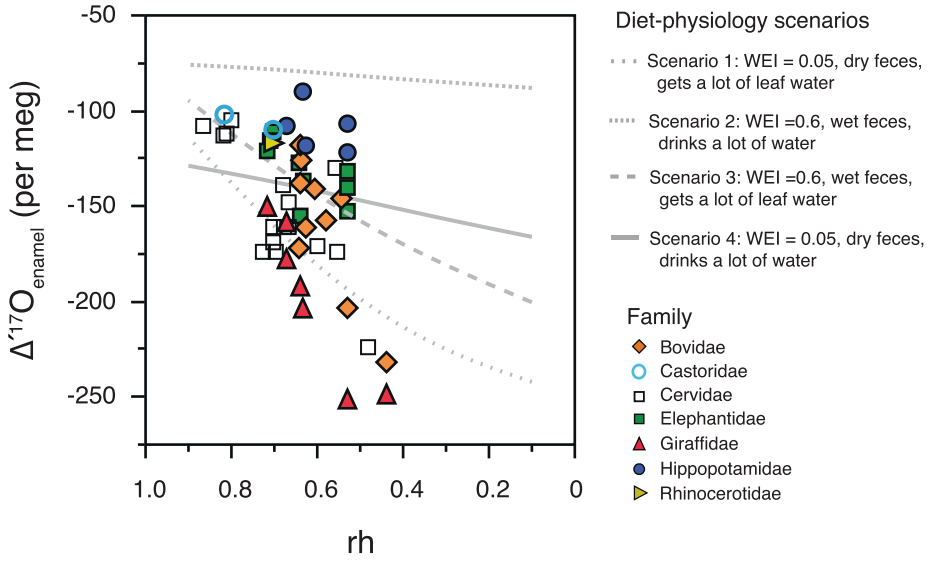

Fig. 5. Observed $\Delta'^{17}O_{enamel}$ values from this study compared to how modeled outputs of $\Delta'^{17}O_{enamel}$ values vary with relative humidity (rh), based on a version of the Kohn (1996) model that is modified for triple oxygen isotopes (Passey and Levin, 2021). Each line represents modeled outputs using different diet-physiology scenarios (Scenarios 1 – 4), where Water Economy Index, feces water content, and drinking water amounts vs. leaf water consumption are varied. Modeled body water $\Delta'^{17}O$ values are converted to $\Delta'^{17}O_{enamel}$ assuming $^{18/16}\alpha_{enamel\text{-}body\ water} = 1.0244$ using the approaches outlined in Passey and Levin (2021) and Lécuyer et al. (2010) and assuming $\theta_{enamel\text{-}body\text{-}water} = 0.525$. See Section 4.1.2 for references and further discussion.

to characterize environment of a particular place during average conditions (Supplementary Table 7).

For comparison to our $\Delta'^{17}O_{enamel}$ results, we convert the outputs for body water $\Delta'^{17}O$ values to the equivalent mineral (enamel carbonate) composition using the approaches outlined in Passey and Levin (2021) (Fig. 5). We calculate $\Delta'^{17}O_{enamel}$ from modeled body water $\Delta'^{17}O$ values ($\Delta'^{17}O_{body\ water}$) using the following relationship.

$$^{17}\alpha_{enamel-body\ water} = \left(^{18}\alpha_{enamel-body\ water}\right)^{\theta}, \quad (5)$$

For the purposes of these calculations, we assume the triple oxygen isotope fractionation between body water and enamel ($\theta_{enamel\text{-}body\text{-}water}$) is 0.525 and similar to the relationship for water and calcite ($\theta_{calcite\text{-}water}$), which ranges between 0.525 and 0.526 based on theoretical and experimental estimates for Earth surface conditions (e.g., Cao and Liu, 2011; Passey et al., 2014; Hayles et al., 2018; Guo and Zhou, 2019; Wostbrock et al., 2020b; Schauble and Young, 2021; Sharp and Wostbrock, 2021). Further work is needed to determine specific values for $\theta_{enamel\text{-}body\text{-}water}$ for enamel carbonate. We use

Please cite this article in press as: Lehmann S. B., et al. Triple oxygen isotope distribution in modern mammal teeth and potential geologic applications. *Geochim. Cosmochim. Acta* (2022), https://doi.org/10.1016/j.gca.2022.04.033

$^{18}\alpha_{\text{enamel-body water}}$ of 1.0224 assuming body water of 38 °C (i.e., the temperature at which biominerals form) (Lécuyer et al., 2010; Passey et al., 2014). We then calculate $^{17}\alpha_{\text{enamel-body water}}$ from $^{18}\alpha_{\text{enamel-body water}}$ and $\theta_{\text{enamel-body-water}}$ and calculate $\Delta'^{17}O_{\text{enamel}}$ values accordingly. See Section 1.2 for the explanation of terms.

The model results from the four scenarios mostly plot within the range in $\Delta'^{17}O_{\text{enamel}}$ values that we observed (Fig. 5). The standard evaporation-sensitive scenario (Scenario 1) captures minimum $\Delta'^{17}O$ values that decrease in more arid conditions (low relative humidity), whereas the maximum water dependency model (Scenario 2) captures the upper range of $\Delta'^{17}O_{\text{enamel}}$ values where there is little variation with aridity. The outputs from Scenarios 3 and 4 represent variants of Scenarios 1 and 2, with different combinations of Water Economy Index and leaf-water consumption; correspondingly, they yield $\Delta'^{17}O_{\text{enamel}}$ values that plot between those from Scenarios 1 and 2. Changing the Water Economy Index adjusts the relative value of $\Delta'^{17}O_{\text{enamel}}$ (low Water Economy Index matches low $\Delta'^{17}O_{\text{enamel}}$), whereas adjusting the proportion of leaf water consumed, changes the sensitivity of $\Delta'^{17}O_{\text{enamel}}$ to relative humidity (consumption of more leaf water increases sensitivity to relative humidity).

The combination of modeled scenarios shows that 1) more water-efficient (low Water Economy Index) animals, such as giraffe and deer, should have lower $\Delta'^{17}O_{\text{enamel}}$ values than less water-efficient animals (high Water Economy Index) like hippos and beavers (Fig. 5) and 2) $\Delta'^{17}O_{\text{enamel}}$ values should decrease with increasing aridity, especially for animals with low Water Economy Index, given the greater reliance of water-efficient animals on evaporated and low $\Delta'^{17}O$ water sources (e.g., leaf and plant water) in water-stressed, arid environments. These outputs capture the trends in the observed $\Delta'^{17}O_{\text{enamel}}$ data; evaporation-sensitive taxa yield lower $\Delta'^{17}O_{\text{enamel}}$ values than evaporation-insensitive taxa (Fig. 4A) and $\Delta'^{17}O_{\text{enamel}}$ values decrease with increased aridity (Figs. 3, 5). The model-data comparison here confirms the strong influences of both diet and physiology and environment on $\Delta'^{17}O_{\text{enamel}}$ values identified by Passey and Levin (2021). $\Delta'^{17}O_{\text{enamel}}$ varies within a guild of mammals in a single environment, due to differences in behavior, physiology, water-use strategy, and also across environments.

4.2. Applying $\Delta'^{17}O_{\text{enamel}}$ from large mammalian herbivores to reconstruct past aridity

Considering the generalized $\Delta'^{17}O_{\text{enamel}}$ – aridity relationship among extant animals, across a range of geographic and climate settings, we suggest that $\Delta'^{17}O_{\text{enamel}}$ of fossils can be used to assess past aridity. In the following text we discuss the use of $\Delta'^{17}O_{\text{enamel}}$ values of fossil mammalian herbivores as an indicator of past aridity and the advantages to using $\Delta'^{17}O_{\text{enamel}}$ values rather than approaches that rely on $\delta^{18}O_{\text{enamel}}$ alone.

4.2.1. $\Delta'^{17}O_{\text{enamel}}$ as an indicator of aridity

The $\Delta'^{17}O_{\text{enamel}}$ data from modern mammalian herbivores plot in a wedge-shaped pattern with AI that is consistent across geographic regions and among different taxa; the variance in $\Delta'^{17}O_{\text{enamel}}$ values is greatest in more arid environments. Translating this to the fossil record means that variations of $\Delta'^{17}O_{\text{enamel}}$ values from fossil assemblages may be used to infer relative differences in aridity between sites, such that sites with greater variance in $\Delta'^{17}O_{\text{enamel}}$ values represent more arid conditions than sites where $\Delta'^{17}O_{\text{enamel}}$ values are tightly clustered.

When using $\Delta'^{17}O_{\text{enamel}}$ values of fossils to compare aridity between sites and through time, sample sets should include taxa from the full range of water-use strategies available in a fossil assemblage. This increases the chances for $\Delta'^{17}O_{\text{enamel}}$ values in the sample set to capture the range in $\Delta'^{17}O_{\text{enamel}}$ values among a population from one place. In our study of extant mammals, we targeted teeth from animals with a range of water-use strategies from each site, but limited our analysis to only two samples for many sites to keep the analytical scope of the project manageable (e.g., hippopotamids/elephantids vs. giraffids) (Table 2). Even with limited sampling, we observe greater variation in $\Delta'^{17}O_{\text{enamel}}$ values with increasing aridity. We would likely observe a greater variation in $\Delta'^{17}O_{\text{enamel}}$ values with bigger sample sizes, meaning that the variation in $\Delta'^{17}O_{\text{enamel}}$ values from any place would only provide an indication of minimum aridity for a site.

In the most basic sense, $\Delta'^{17}O_{\text{enamel}}$ values of fossil teeth can be used to gauge relative differences in aridity between fossil sites. However, $\Delta'^{17}O_{\text{enamel}}$ values from fossils can also be considered in terms of the UNESCO climate classifications arid, semi-arid, subhumid, and humid. Pooling our observations from three continents, the expected ranges for $\Delta'^{17}O_{\text{enamel}}$ values from guilds of mammalian herbivores are approximately 75 per meg in humid climates, 135 per meg in semi-arid climates, and 145 per meg in arid climates (Fig. 3B, 3E). We expect adjustments to these values as more individuals, taxa, and environments are sampled and added to this global dataset.

4.2.2. Advantages of using $\Delta'^{17}O$ as an aridity indicator compared to using $\delta^{18}O_{\text{enamel}}$ alone

The relationship between $\Delta'^{17}O_{\text{enamel}}$ values and aridity is compelling as a paleoaridity indicator because it persists across a wide range of sites, with varying geography and $\delta^{18}O$ values of meteoric water, and among different combinations of mammalian taxa. In contrast, we do not observe similarly clear relationships between $\delta^{18}O_{\text{enamel}}$ values and aridity because $\delta^{18}O_{\text{enamel}}$ values are influenced by many other parameters in addition to aridity. This mirrors what we observe in waters: $\delta^{18}O$ values of waters are sensitive to a myriad of geographic and climatic parameters (e.g., elevation, temperature, continentality, precipitation amount, evaporative water loss), whereas evaporation dominates the variation of $\Delta'^{17}O$ values in water (see Aron et al. (2021) for a recent review). As such, $\delta^{18}O_{\text{enamel}}$ based reconstructions of aridity depend on the identification of taxa that fit into clear evaporation-sensitive and evaporation-insensitive categories to control for the varying isotopic composition of local waters, but this limits the extent of its application (e.g., Blumenthal et al., 2017).

Please cite this article in press as: Lehmann S. B., et al. Triple oxygen isotope distribution in modern mammal teeth and potential geologic applications. *Geochim. Cosmochim. Acta* (2022), https://doi.org/10.1016/j.gca.2022.04.033

4.3. Other geological applications for $\Delta'^{17}O_{enamel}$ of large mammalian herbivores

4.3.1. Past pCO_2

We are not aware of other studies that propose the use of $\Delta'^{17}O_{enamel}$ values as indicators of paleoaridity, but a handful of recent studies have suggested the use of $\Delta'^{17}O$ values from teeth and eggshells to constrain past atmospheric pCO_2 and past gross primary productivity (GPP) (Pack et al., 2013; Passey et al., 2014; Gehler et al., 2016; Passey and Levin, 2021). This is an exciting development given the importance of understanding the history of Earth's pCO_2 and global GPP. This approach has been applied to reconstruct pCO_2 across the Paleocene–Eocene Thermal Maximum (PETM); Gehler et al. (2016) use a 60 per meg decrease in $\Delta'^{17}O_{enamel}$ values across the PETM to infer a ca. 400 to 1000 ppm increase in atmospheric pCO_2. This approach works because inhaled atmospheric O_2, which has a $\Delta'^{17}O$ value considerably lower than any form of water (Fig. 1), contributes between 5% to 40% of mammalian body water oxygen. As such, the $\Delta'^{17}O$ value of atmospheric O_2 is apparent in tooth enamel $\Delta'^{17}O$ values; it pushes the $\Delta'^{17}O$ values of body water and enamel more negative than the influences of food and drinking water oxygen alone (Pack et al., 2013). The $\Delta'^{17}O$ value of atmospheric O_2 is influenced by mass independent fractionation of oxygen isotopes in the stratosphere, where higher concentrations of atmospheric CO_2 leads to decreased $\Delta'^{17}O$ values of atmospheric O_2 (Luz et al., 1999; Bao et al., 2008), and in turn, lower $\Delta'^{17}O_{enamel}$ values (Pack et al., 2013). The measured relationship between the $\Delta'^{17}O$ (O_2) – pCO_2 is linear at low pCO_2 (slope ~ -2.0) such that for every 100 ppm increase in pCO_2, there is a commensurate 20 per meg decrease in $\Delta'^{17}O$ of atmospheric O_2 (Luz et al., 1999); we note that this relationship has been modeled as slightly non-linear when $pCO_2 \gtrsim 10{,}000$ ppm (Bao et al., 2008).

Currently, $\Delta'^{17}O_{enamel}$-based estimates of pCO_2 are calculated from animals with small body mass and high respiration rates (Gehler et al., 2016). These estimates do not consider how $\Delta'^{17}O_{enamel}$ values vary among taxa (aside from differences in body mass) or in different environments. But such variation is important; a 60 per meg distinction in $\Delta'^{17}O_{enamel}$ values that is used to infer changes in pCO_2 can also be observed within an arid location among different animals (e.g., Turkana) or between environments (e.g., 60 per meg represents the difference between a subhumid and arid environment; Fig. 3). Given the similar magnitude of change in $\Delta'^{17}O_{enamel}$ values that occurs with a change in environment, animal taxon, or pCO_2, it will be essential to characterize the influence of environment on $\Delta'^{17}O_{enamel}$ values of mammalian herbivores before using them to infer pCO_2. To do this, we suggest sampling teeth from a range of taxa and from multiple fossil sites within a single time interval. Sites from a single time period across the globe should have similar atmospheric pCO_2. If pCO_2 is significantly different from today, then there will be a wholesale shift in $\Delta'^{17}O_{enamel}$ values away from the modern distribution of $\Delta'^{17}O_{enamel}$ values across multiple fossil sites, environments, and populations of taxa. We recognize that assessing past pCO_2 using $\Delta'^{17}O_{enamel}$ will require further study, but any use of $\Delta'^{17}O_{enamel}$ as a proxy for CO_2 needs to consider environmental and taxonomic variation in $\Delta'^{17}O_{enamel}$ values.

4.3.2. Diagenesis

Assessing and accounting for the role of diagenesis on $\delta^{18}O$ values of biological carbonate (i.e., tooth, bone, eggshell) has been a longstanding challenge in their use for paleoclimate reconstructions (e.g., Iacumin et al., 1996; Schoeninger et al., 2003). Any post-depositional reprecipitation of carbonate reflects the temperatures and isotopic composition of waters of this secondary event, not the biomineralization in an animal. The influence of reprecipitated carbonate on $\delta^{18}O_{enamel}$ values can be evaluated by comparing $\delta^{18}O_{enamel}$ values among different taxa, the $\delta^{18}O$ of phosphate in the same tooth enamel, or to the $\delta^{18}O$ of sedimentary carbonates. Analysis of the elemental composition of bioapatite using x-ray diffraction and infrared spectroscopy is another approach (e.g., Person et al., 1995; Iacumin et al., 1996).

The triple oxygen isotope composition of carbonates and bioapatites provides an additional way to evaluate the effects of diagenesis (Gehler et al., 2011). Biological carbonate and apatite $\Delta'^{17}O$ values are more negative and more variable than the $\Delta'^{17}O$ values of carbonates derived from meteoric waters due to the influence of low-$\Delta'^{17}O$ inhaled atmospheric O_2 and the strong roles of environment and animal water-use that results in varying $\Delta'^{17}O$ values (Fig. 6).

The clear distinction between $\Delta'^{17}O$ values of biological carbonates and meteoric carbonates means that $\Delta'^{17}O$ measurements can be used to evaluate diagenesis of the original oxygen isotopic composition of biological carbonate without relying on additional analyses and materials. Gehler et al. (2011) suggests the $\Delta'^{17}O$ values of tissue from small mammals (<1 kg) can help evaluate diagenesis based on this distinction; biological carbonates incorporate highly negative $\Delta'^{17}O$ values from inhaled O_2 whereas meteoric carbonates do not. While this approach was initially presented for small animals, given their high metabolic rates, this concept is also relevant for larger mammals (>6 kg) and birds, as $\Delta'^{17}O$ values of tooth enamel and eggshells are more negative and more variable than those of meteoric-derived carbonates (Fig. 6). There are some exceptions; carbonates formed from waters that are extensively evaporated, such as closed basin, saline Mono Lake, can have $\Delta'^{17}O$ values as low as −214 per meg (see Passey and Ji, 2019) and fall squarely in the range of $\Delta'^{17}O$ values of bird and mammal carbonate.

To use $\Delta'^{17}O$ analyses to determine diagenesis of fossil enamel, a sample set should include both fossils from taxa with a range of water-use strategies and carbonates that are available from the sediments associated with the fossils (e.g., soil carbonate, lacustrine carbonate, cements). If the $\Delta'^{17}O_{enamel}$ values are unaltered, then they will be more negative and varied than that of the associated carbonates. If the $\Delta'^{17}O$ values of sedimentary carbonates and enamel are similar, then the distribution of $\Delta'^{17}O_{enamel}$ values will be compressed and the original oxygen isotopic

Please cite this article in press as: Lehmann S. B., et al. Triple oxygen isotope distribution in modern mammal teeth and potential geologic applications. *Geochim. Cosmochim. Acta* (2022), https://doi.org/10.1016/j.gca.2022.04.033

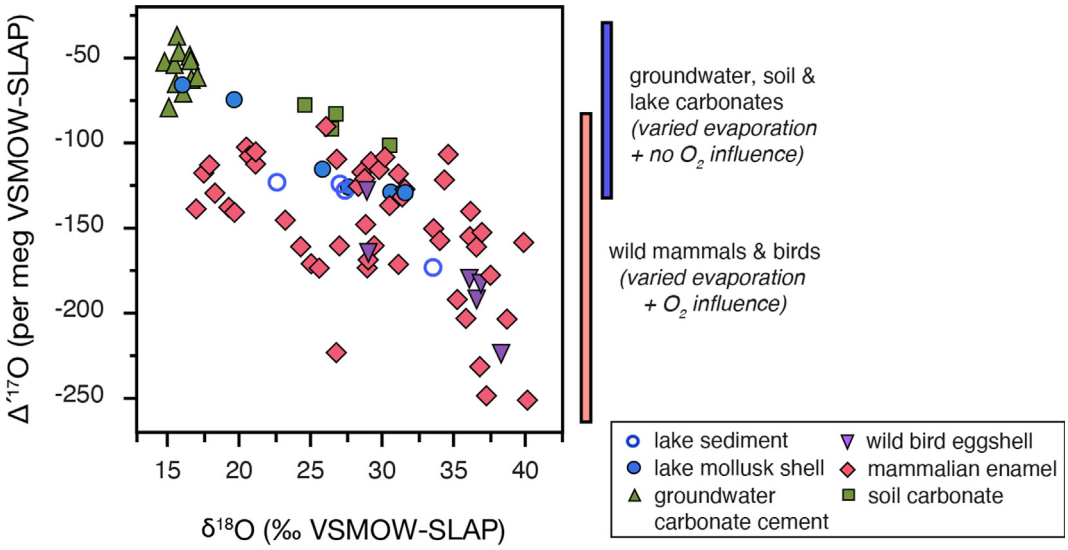

Fig. 6. The $\Delta'^{17}O$ and $\delta^{18}O$ values of large mammalian tooth enamel, bird eggshells, mollusks, and groundwater cement, lake, and soil carbonates. Data are from Passey et al. (2014), Passey and Ji (2019), and this study.

composition of the fossil teeth has been altered. This concept can be extended to other fossil biological carbonate like bones and eggshells.

We note that Wostbrock et al. (2020b) provide an approach for evaluating the impacts of diagenesis on marine carbonates to reconstruct the $\Delta'^{17}O$ values of the primary carbonate. While this approach works in marine settings, we cannot readily translate it to bioapatite from terrestrial settings as it relies on knowledge (or assumption) of the $\delta^{18}O$ value of the primary formation water (the ocean for marine carbonates), but we cannot assume a value for the $\delta^{18}O$ of the body water from which bioapatite initially forms.

5. CONCLUSIONS

The $\Delta'^{17}O_{enamel}$ values of extant, large mammalian herbivores sampled from three continents and seven mammalian families vary by 162 per meg (–252 to −90 per meg). The relationship between $\Delta'^{17}O_{enamel}$ values and aridity form a wedge-shaped pattern, with greater variation in $\Delta'^{17}O_{enamel}$ values in arid environments. This relationship is independent of latitude and $\delta^{18}O$ value of local meteoric waters. However, the relationship between $\Delta'^{17}O_{enamel}$ values does depend on animal water-use strategy; generally, $\Delta'^{17}O_{enamel}$ values from water-dependent animals vary little with aridity, whereas water-efficient animals yield lower $\Delta'^{17}O_{enamel}$ values that decrease with aridity.

Our dataset provides a framework for using $\Delta'^{17}O_{enamel}$ values to evaluate aridity of past environments. The $\Delta'^{17}O_{enamel}$ values from multiple taxa in a fossil assemblage can be used to estimate the paleoaridity of a fossil site and roughly place it into one of the UNESCO climate categories. The use of $\Delta'^{17}O_{enamel}$ values broadens the utility of the oxygen isotope composition of terrestrial materials for paleoenvironmental reconstructions because their distribution is strongly tied to aridity, unlike $\delta^{18}O$ values of enamel (and other materials) which are influenced by a combination of multiple factors in addition to aridity (e.g., temperature, $\delta^{18}O$ values of meteoric water).

In addition to their utility for paleoenvironmental reconstructions, $\Delta'^{17}O$ values of fossil teeth may potentially be used to estimate past pCO_2 and evaluate diagenetic effects on the oxygen isotope composition of samples. Our expanded dataset from extant herbivores shows the importance of sampling teeth from a range of taxa for both of these approaches to work effectively. Studies that use $\Delta'^{17}O_{enamel}$ values as a pCO_2 indicator must first account for the range of $\Delta'^{17}O_{enamel}$ variation due to the environment and animal water-use strategy. Likewise, any study using $\Delta'^{17}O_{enamel}$ values to identify diagenesis should include samples from taxa with different water-use strategies because they should yield $\Delta'^{17}O_{enamel}$ values that are relatively wide-ranging if unaltered and relatively invariant if altered. These results show the expanded potential for the utility of triple oxygen isotope distributions in biocarbonates. The next steps for this work include expanding the sample from extant animals to include more individuals from a broader range of geographic settings and then applying this framework to constrain aridity, pCO_2, and diagenesis in Earth's past.

Declaration of Competing Interest

The authors declare that they have no known competing financial interests or personal relationships that could have appeared to influence the work reported in this paper.

ACKNOWLEDGEMENTS

We thank David Patterson, Scott Blumenthal, and staff from the Edness Kimball Wilkins State National Park, WY for

providing samples for analysis. Many of these samples reflect collections made as part of monitoring and conserving wild mammal populations and we are grateful to the many people who are committed to these long-term efforts. We also thank Scott Blumenthal for sharing his Matlab code for extracting climate information from each site and for assistance in extracting climate information for each site. We appreciate the efforts of the reviewers and the Associate Editor whose constructive comments substantially strengthened the manuscript. We thank the Department of Earth and Planetary Sciences Department at Johns Hopkins University where samples were prepared and analyzed. Postdoctoral fellowships from the National Science Foundation supported Emily Beverly and Julia Kelson (EAR-PF 1725621, EAR-PF 1854873) for their work on this paper. A Johns Hopkins Early Career Catalyst Grant awarded to Naomi Levin funded this work.

APPENDIX A. SUPPLEMENTARY MATERIAL

Supplementary material to this article can be found online at https://doi.org/10.1016/j.gca.2022.04.033.

REFERENCES

Alexandre A., Landais A., Vallet-Coulomb C., Piel C., Devidal S., Pauchet S., Sonzogni C., Couapel M., Pasturel M., Cornuault P., Xin J., Mazur J.-C., Prié F., Bentaleb I., Webb E., Chalié F. and Roy J. (2018) The triple oxygen isotope composition of phytoliths as a proxy of continental atmospheric humidity: insights from climate chamber and climate transect calibrations. *Biogeosciences* **15**, 3223–3241.

Aron P. G., Levin N. E., Beverly E. J., Huth T. E., Passey B. H., Pelletier E. M., Poulsen C. J., Winkelstern I. Z. and Yarian D. A. (2021) Triple oxygen isotopes in the water cycle. *Chem. Geol.* **565** 120026.

Bao H., Lyons J. R. and Zhou C. (2008) Triple oxygen isotope evidence for elevated CO_2 levels after a Neoproterozoic glaciation. *Nature* **453**, 504–506.

Barkan E. and Luz B. (2005) High precision measurements of $^{17}O/^{16}O$ and $^{18}O/^{16}O$ ratios in H_2O. *Rapid Commun. Mass Spectrom.* **19**, 3737–3742.

Barkan E. and Luz B. (2007) Diffusivity fractionations of $H_2^{16}O/H_2^{17}O$ and $H_2^{16}O/H_2^{18}O$ in air and their implications for isotope hydrology. *Rapid Commun. Mass Spectrom.* **21**, 2999–3005.

Barkan E. and Luz B. (2011) The relationships among the three stable isotopes of oxygen in air, seawater and marine photosynthesis. *Rapid Commun. Mass Spectrom.* **25**, 2367–2369.

Blumenthal S. A., Levin N. E., Cerling T. E., Brown F. H., Brugal J.-P., Chritz K. L., Harris J. M. and Jehle G. E. (2017) Aridity and early hominin environments. *Proc. Natl. Acad. Sci. U.S.A.* **114**, 7331–7336.

Bowen G. J. and Revenaugh J. (2003) Interpolating the isotopic composition of modern meteoric precipitation. *Water Resour. Res.* **39**, 1299.

Brand W. A., Coplen T. B., Vogl J., Rosner M. and Prohaska T. (2014) Assessment of international reference material for isotope-ratio analysis (IUPAC Technical Report). *Pure Appl. Chem.* **82**, 1719–1733.

Bryant J. D., Koch P. L., Froelich P. N., Showers W. J. and Genna B. J. (1996) Oxygen isotope partitioning between phosphate and carbonate in mammalian apatite. *Geochim. Cosmochim. Acta* **60**, 5145–5148.

Bryant J. D. and Froelich P. N. (1995) A model of oxygen isotope fractionation in body water of large mammals. *Geochim. Cosmochim. Acta* **59**, 4523–4537.

Cao X. B. and Liu Y. (2011) Equilibrium mass–dependent fractionation relationships for triple oxygen isotopes. *Geochim. Cosmochim. Acta* **75**, 7435–7445.

Cerling T. E., Andanje S. A., Blumenthal S. A., Brown F. H., Chritz K. L., Harris J. M., Hart J. A., Kirera F. M., Kaleme P., Leakey L. N., Leakey M. G., Levin N. E., Manthi F. K., Passey B. E. and Uno K. T. (2015) Dietary changes of large herbivores in the Turkana Basin, Kenya from 4 to 1 Ma. *Proc. Natl. Acad. Sci. U.S.A.* **112**, 11467–11472.

Cerling T. E., Harris J. M., Hart J. A., Kaleme P., Klingel H., Leakey M. G., Levin N. E., Lewison R. L. and Passey B. H. (2008) Stable isotope ecology of the common hippopotamus. *J. Zool.* **276**, 204–212.

Cerling T. E., Harris J. M. and Passey B. H. (2003) Diets of East African Bovidae based on stable isotope analysis. *J. Mamm.* **84** (2), 456–470.

Cerling T. E., Hart J. A. and Hart T. B. (2004) Stable isotope ecology in the Ituri Forest. *Oecologia* **138**, 5–12.

Cerling T. E., Harris J. M. and Leakey M. G. (1999) Browsing and grazing in elephants: the isotope record of modern and fossil proboscideans. *Oecologia* **120**, 364–374.

Craig H. (1957) Isotopic standards for carbon and oxygen and correction factors for mass-spectrometric analysis of carbon dioxide. *Geochim. Cosmochim. Acta* **12**, 133–149.

Dansgaard W. (1964) Stable Isotopes in Precipitation. *Tellus* **16**, 436–468.

Fricke H. C., O'Neil J. R. and Lynnerup N. (1995) Oxygen isotope composition of human tooth enamel from Medieval Greenland: linking climate and society. *Geology* **23**, 869–872.

Gehler A., Gingerich P. D. and Pack A. (2016) Temperature and atmospheric CO_2 concentration estimates through the PETM using triple oxygen isotope analysis of mammalian bioapatite. *Proc. Natl. Acad. Sci. U.S.A.* **113**, 7739–7744.

Gehler A., Tütken T. and Pack A. (2011) Triple oxygen isotope analysis of bioapatite as tracer for diagenetic alteration of bones and teeth. *Palaeogeogr. Palaeoclim. Palaeoecol.* **310**, 84–91.

Guo W. and Zhou C. (2019) Triple oxygen isotope fractionation in the DIC–H_2O–CO_2 system: A numerical framework and its implications. *Geochim. Cosmochim. Acta* **246**, 541–564.

Hayles J., Gao C., Cao X., Liu Y. and Bao H. (2018) Theoretical calibration of the triple oxygen isotope thermometer. *Geochim. Cosmochim. Acta* **235**, 237–245.

Herwartz D., Surma J., Voigt C., Assonov S. and Staubwasser M. (2017) Triple oxygen isotope systematics of structurally bonded water in gypsum. *Geochim. Cosmochim. Acta* **209**, 254–266.

Hijmans R. J., Cameron S. E., Parra J. L., Jones P. G. and Jarvis A. (2005) Very high resolution interpolated climate surfaces for global land areas. *Int. J. Climatol.* **25**, 1965–1978.

Hoppe K. A. (2006) Correlation between the oxygen isotope ratio of North American bison teeth and local waters: Implication for paleoclimatic reconstructions. *Earth Planet. Sci. Lett.* **244**, 408–417.

Iacumin P., Bocherens H., Mariotti A. and Longinelli A. (1996) Oxygen isotope analyses of co-existing carbonate and phosphate in biogenic apatite: a way to monitor diagenetic alteration of bone phosphate?. *Earth Planet Sci. Lett.* **142** 1–6.

Kohn M. J. (1996) Predicting animal $\delta^{18}O$: accounting for diet and physiological adaptation. *Geochim. Cosmochim. Acta* **60**, 4811–4829.

Landais A., Barkan E., Yakir D. and Luz B. (2006) The triple isotopic composition of oxygen in leaf water. *Geochim. Cosmochim. Acta* **70**, 4105–4115.

Landais A., Risi C., Bony S., Vimeux F., Descroix L., Falourd S. and Bouygues A. (2010) Combined measurement of ^{17}O-excess and d-excess in African monsoon precipitation: Implication for

evaluating convective parameterizations. *Earth Planet. Sci. Lett.* **298**, 104–112.

Lécuyer C., Balter V., Martineau F., Fourel F., Bernard A., Amiot R., Gardien V., Otero O., Legendre S., Panczer G., Simon L. and Martini R. (2010) Oxygen isotope fractionation between apatite–bound carbonate and water determined from controlled experiments with synthetic apatites precipitated at 10–37C. *Geochim. Cosmochim. Acta* **74**, 2072–2081.

Levin N. E., Cerling T. E., Passey B. H., Harris J. M. and Ehleringer J. R. (2006) A stable isotope aridity index for terrestrial environments. *Proc. Natl. Acad. Sci. U.S.A.* **103**, 11201–11205.

Levin N. E., Simpson S. W., Quade J., Cerling T. E. and Frost S. R. (2008) Herbivore enamel carbon isotopic composition and the environmental context of Ardipithecus at Gona, Ethiopia. In *The Geology of Early Humans in the Horn of Africa* (eds. J. Quade and J. G. Wynn). Geological Society of America, Boulder, CO, pp. 215–234.

Li S., Levin N. E., Soderberg K., Dennis K. J. and Caylor K. K. (2017) Triple oxygen isotope composition of leaf waters in Mpala, central Kenya. *Earth Planet. Sci. Lett.* **468**, 38–50.

Luyt J., Hare V. J. and Sealy J. (2019) The relationship of ungulate $\delta^{13}C$ and environment in the temperate biome of southern Africa, and its palaeoclimatic application. *Palaeogeogr. Palaeoclim. Palaeoecol.* **514**, 282–291.

Luz B., Cormie A. B. and Schwarcz H. P. (1990) Oxygen isotope variations in phosphate of deer bones. *Geochim. Cosmochim. Acta* **54**, 1723–1728.

Luz B., Barkan E., Bender M. L., Thiemens M. H. and Boering K. A. (1999) Triple–isotope composition of atmospheric oxygen as a tracer of biosphere productivity. *Nature* **400**, 547–550.

Luz B. and Barkan E. (2010) Variations of $^{17}O/^{16}O$ and $^{18}O/^{16}O$ in meteoric waters. *Geochim. Cosmochim. Acta* **74**, 6276–6286.

Matsuhisa Y., Goldsmith J. R. and Clayton R. N. (1978) Mechanisms of hydrothermal crystallization of quartz at 250C and 15kbar. *Geochim. Cosmochim. Acta* **42**, 173–182.

Miller M. F. (2002) Isotopic fractionation and the quantification of ^{17}O anomalies in the oxygen three–isotope system: an appraisal and geochemical significance. *Geochim. Cosmochim. Acta* **66**, 1881–1889.

Nagy K. A. and Peterson C. C. (1988) Scaling of water flux rate in animals. *Univ. Calif. Publ. Zool.* **120**, 1–172.

New M., Lister D., Hulme M. and Makin I. (2002) A high-resolution data set of surface climate over global land areas. *Clim. Res.* **21**, 1–25.

Nowak R. (1999) *Walker's Mammals of the World*, Sixth Edition. The Johns Hopkins University Press, Baltimore, MD.

Pack A. (2021) Isotopic traces of atmospheric O_2 in rocks, minerals, and melts. *Rev. Mineral. Geochem.* **86**, 217–240.

Pack A., Gehler A. and Süssenberger A. (2013) Exploring the usability of isotopically anomalous oxygen in bones and teeth as paleo–CO_2–barometer. *Geochim. Cosmochim. Acta* **102**, 306–317.

Passey B. H. and Levin N. E. (2021) Triple oxygen isotopes in meteoric waters, carbonates, and biological apatites: implications for continental paleoclimate reconstruction. *Rev. Mineral. Geochem.* **86**, 429–462.

Passey B. H., Hu H., Ji H., Montanari S., Li S., Henkes G. A. and Levin N. E. (2014) Triple oxygen isotopes in biogenic and sedimentary carbonates. *Geochim. Cosmochim. Acta* **141**, 1–25.

Passey B. H. and Ji H. (2019) Triple oxygen isotope signatures of evaporation in lake waters and carbonates: A case study from the Western United States. *Earth Planet. Sci. Lett.* **518**, 1–12.

Passey B. H., Cerling T. E. and Levin N. E. (2007) Temperature dependence of oxygen isotope acid fractionation for modern and fossil tooth enamels. *Rapid Commun. Mass Spectrom.* **21**, 2853–2859.

Person A., Bocherens H., Saliège J. F., Paris F., Zeitoun V. and Gérard M. (1995) Early diagenetic evolution of bone phosphate: An x-ray diffractometry analysis. *J. Archaeol. Sci.* **22**, 211–221.

Rowley D. B. and Currie B. S. (2006) Palaeo–altimetry of the late Eocene to Miocene Lunpola basin, central Tibet. *Nature* **439**, 677–681.

Rozanski K., Araguás-Araguás L. and Gonfiantini R. (1993) Isotopic patterns in modern global precipitation. In *Climate Change in Continental Isotopic Records* (eds. P. K. Swart, K. C. Lohmann, J. McKenzie and S. Savin). American Geophysical Union Geophysical Monograph. American Geophysical Union, Washington, DC, pp. 1–36.

Schauble E. A. and Young E. D. (2021) Mass dependence of equilibrium oxygen isotope fractionation in carbonate, nitrate, oxide, perchlorate, phosphate, silicate, and sulfate minerals. *Rev. Mineral. Geochem.* **86**, 137–178.

Schoenemann S. W., Schauer A. J. and Steig E. J. (2013) Measurement of SLAP2 and GISP $\delta^{17}O$ and proposed VSMOW–SLAP normalization for $\delta^{17}O$ and $\delta^{18}O$. *Rapid Commun. Mass Spectrom.* **27**, 582–590.

Schoeninger M. J., Hallin K., Reeser H., Valley J. W. and Fournelle J. (2003) Isotopic alteration of mammalian tooth enamel. *In. J. Osteoarchaeol.* **13**, 11–19.

Sharp Z. D. and Wostbrock J. A. G. (2021) Standardization for the triple oxygen isotope system: Waters, silicates, carbonates, air, and sulfates. *Rev. Mineral. Geochem.* **86**, 179–196.

Surma J., Assonov S., Bolourchi M. J. and Staubwasser M. (2015) Triple oxygen isotope signatures in evaporated water bodies from the Sistan Oasis, Iran. *Geophys. Res. Lett.* **42**, 8456–8462.

Surma J., Assonov S., Herwartz D., Voigt C. and Staubwasser M. (2018) The evolution of ^{17}O-excess in surface water of the arid environment during recharge and evaporation. *Sci. Rep.* **8**, 4972.

Trabucco A., Zomer R. J. (2009) Global Aridity Index (Global-aridity) and Global Potential Evapo-transpiration (Global-PET) Geospatial Database. CGIAR Consortium for Spatial Information. The CGIAR-CSI GeoPortal. http://www.csi.cgiar.org/.

Uechi Y. and Uemura R. (2019) Dominant influence of the humidity in the moisture source region on the ^{17}O-excess in precipitation on a subtropical island. *Earth Planet. Sci. Lett.* **513**, 20–28.

Unesco (1979) *Map of the world distributions of arid regions*. MAB Technical Notes, Paris, France.

Whiteman J. P., Sharp Z. D., Gerson A. R. and Newsome S. D. (2019) Relating $\Delta^{17}O$ values of animal body water to exogenous water inputs and metabolism. *Bioscience* **69**, 658–688.

Wostbrock J. A. G., Cano E. J. and Sharp Z. D. (2020a) An internally consistent triple oxygen isotope calibration of standards for silicates, carbonates and air relative to VSMOW2 and SLAP2. *Chem. Geol.* **533** 119432.

Wostbrock J. A., Brand U., Coplen T. B., Swart P. K., Carlson S. J., Brearley A. J. and Sharp Z. D. (2020b) Calibration of carbonate–water triple oxygen isotope fractionation: Seeing through diagenesis in ancient carbonates. *Geochim. Cosmochim. Acta* **288**, 369–388.

Xu C., Reed R., Gorski J. P., Wang Y. and Walker M. P. (2012) The distribution of carbonate in enamel and its correlation with

Please cite this article in press as: Lehmann S. B., et al. Triple oxygen isotope distribution in modern mammal teeth and potential geologic applications. *Geochim. Cosmochim. Acta* (2022), https://doi.org/10.1016/j.gca.2022.04.033

structure and mechanical properties. *J. Mater. Sci.* **47**, 8035–8043.

Young E. D., Galy A. and Nagahara H. (2002) Kinetic and equilibrium mass–dependent isotope fractionation laws in nature and their geochemical and cosmochemical significance. *Geochim. Cosmochim. Acta* **66**, 1095–1104.

Zachos J., Pagani M., Sloan L., Thomas E. and Billups K. (2001) Trends, rhythms, and aberrations in global climate 65 Ma to present. *Science* **292**, 686–693.

Associate editor: Cedric Michael John